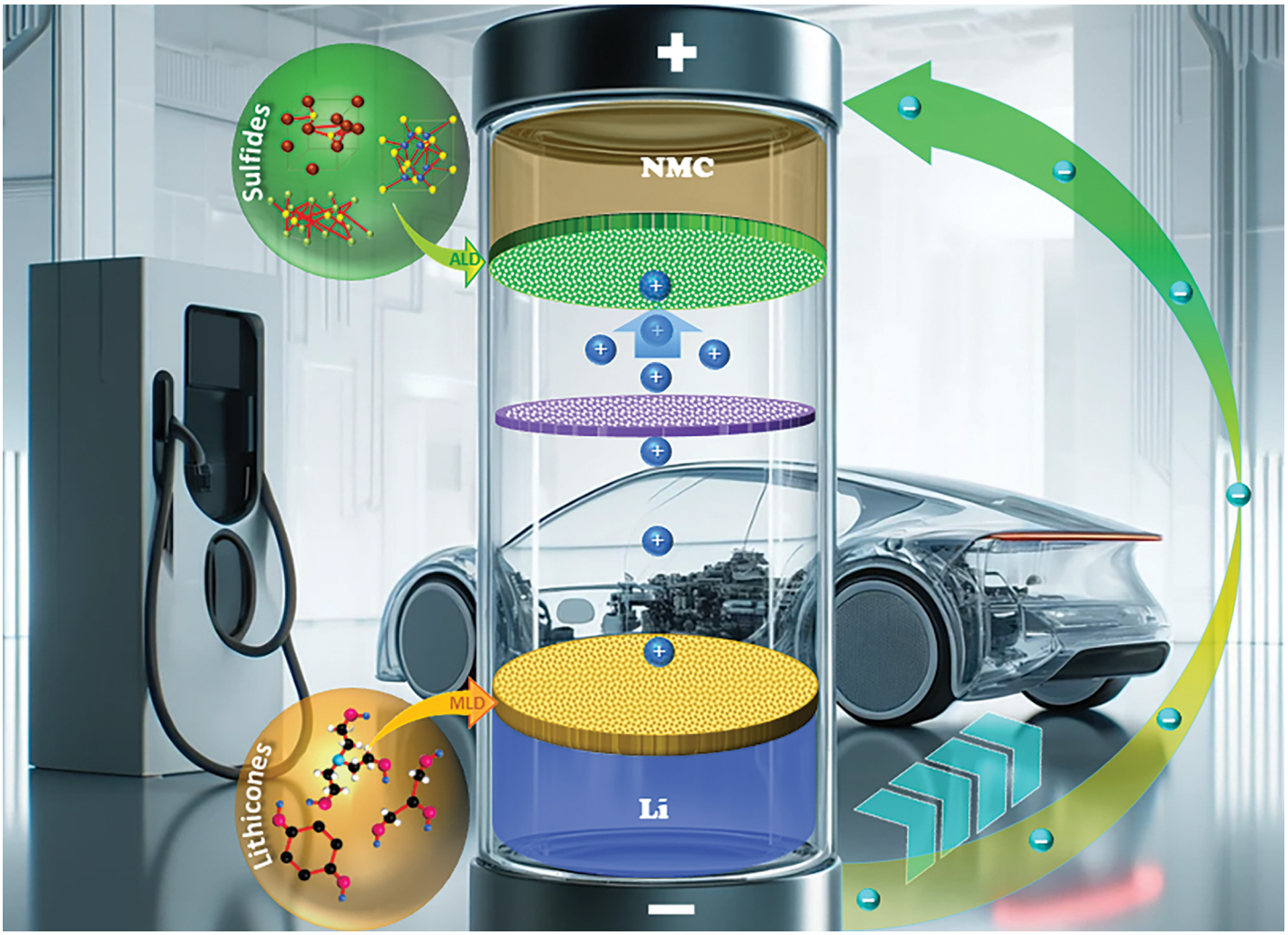

Showcasing research from Professor Xiangbo Meng's laboratory, Department of Mechanical Engineering, University of Arkansas, Fayetteville, the United States.

Accurately constituting robust interfaces for high-performance high-energy lithium metal batteries

By employing novel inorganic sulfide and organic lithicone coatings on lithium metal anodes and NMC cathodes *via* atomic and molecular layer deposition (ALD and MLD), respectively, the performance of the resultant Li||NMC lithium metal batteries has been dramatically improved.

As featured in:

See Xiangbo Meng *et al.*, *Chem. Commun.*, 2025, **61**, 1574.

ROYAL SOCIETY OF CHEMISTRY

rsc.li/chemcomm

Registered charity number: 207890

ChemComm

ROYAL SOCIETY OF CHEMISTRY

FEATURE ARTICLE

View Article Online
View Journal | View Issue

Cite this: *Chem. Commun.*, 2025, **61**, 1574

Accurately constituting robust interfaces for high-performance high-energy lithium metal batteries

Kevin Velasquez Carballo,† Meetesh Singh† and Xiangbo Meng *

High-energy lithium metal batteries (LMBs) have received ever-increasing interest. Among them, coupling lithium metal (Li) with nickel-rich material, $LiNi_xMn_yCo_zO_2$ (NMCs, $x \geq 0.6$, $x + y + z = 1$), is promising because Li anodes enable an extremely high capacity ($\sim$3860 mA h g^{-1}) and the lowest redox potential ($-$3.04 V *vs.* standard hydrogen electrode), while NMCs can achieve a much higher capacity of $\sim$200 mA h g^{-1} and lower cost than those of $LiCoO_2$. However, the resultant Li‖NMC cells have been hindered from commercialization due to a series of challenges related to the interface stability of both Li anodes and NMC cathodes. Specifically, Li anodes suffer from Li dendritic growth and the formation of solid electrolyte interphase (SEI), while NMC cathodes suffer from the formation of cathode electrolyte interphase (CEI) and other interface-related issues, including transition metal dissolution, oxygen release, cracking, and so on. To tackle these issues, recently, two sister techniques, atomic and molecular layer deposition (ALD and MLD), have emerged and exhibit tremendous capabilities to accurately constitute robust interfaces to achieve high-performance Li‖NMC LMBs. They can uniquely develop uniform and conformal films as surface coatings of LMBs in a precisely controllable mode at the atomic/molecular level, while proceeding with film deposition at low temperatures (*e.g.*, $\leq$250 °C). In this Feature Article, we review the latest research progress in developing novel surface coatings *via* ALD and MLD for Li‖NMC LMBs and discuss outcomes for pursuing high performance.

Received 26th October 2024,
Accepted 12th December 2024

DOI: 10.1039/d4cc05705h

rsc.li/chemcomm

1. Introduction

In the 1990s, Sony introduced the first lithium-ion batteries (LIBs) to the market which experienced exceptionally rapid growth thereafter.[1] Nowadays, LIBs dominate portable electronics

Department of Mechanical Engineering, University of Arkansas, Fayetteville, AR 72701, USA. E-mail: xbmeng@uark.edu
† The authors contribute equally.

Kevin Velasquez Carballo

Mr Kevin Velasquez Carballo is a PhD student of Mechanical Engineering at the University of Arkansas, USA, working as a research assistant under the supervision of Dr Xiangbo Meng (2022-present). He earned his bachelor's degree from the same department in 2021. His research focuses on developing high-energy lithium metal batteries using NMC811 cathodes and lithium metal anodes.

Meetesh Singh

Dr Meetesh Singh is a postdoctoral researcher with Dr Xiangbo Meng in the Department of Mechanical Engineering at the University of Arkansas, USA (September 2023-present). He earned his PhD in Condensed Matter Physics from the Indian Institute of Technology, Roorkee, in 2022. He also holds an MS (2013) and a BS (2011) in Physics from H. N. B. Garhwal University, India. His research focuses on alkali metal ion batteries, including lithium, sodium, and potassium-based systems.

and have penetrated the market for electric vehicles (EVs). The wide implementation of LIBs can reduce our dependency on traditional fossil fuels and promise us sustainable prosperity. In pursuing such a goal, however, LIBs currently remain insufficient in their energy density ($\sim$250 W h kg^{-1}) and cost ($\sim$\$170 kW h^{-1}) for EVs.[2–4] According to the US Advanced Battery Consortium and the US National Energy Policy, it is desirable for an EV battery technology to achieve 350 W h kg^{-1} and \$75 kW h^{-1}.[5] To this end, lithium metal batteries (LMBs) have been under intensive investigation, where lithium metal (Li) is adopted as the anode to enable an extremely high capacity ($\sim$3860 mA h g^{-1}) that is over 10 times that of the widely used LIB anode, *i.e.*, graphite (372 mA h g^{-1}). Additionally, Li anodes have a low redox potential, -3.04 V *vs.* standard hydrogen electrode (SHE). Depending on the cathodes used to couple with Li anodes, the resultant LMBs differ in their energy density and have the potential to reach 500 W h kg^{-1} or higher.[6–8] Specifically, for instance, Li anodes could couple with existing metal oxide cathodes of LIBs (such as $LiNi_xMn_yCo_zO_2$ (NMCs, $x + y + z = 1$)) or emerging cathodes, such as sulfur (S) and oxygen (O_2), to constitute LMBs.[9–11] Typically, a liquid electrolyte (LE) is used in LMBs, but recently there has been an increasing interest in solid-state electrolytes (SEs). Although very promising, LMBs have not been commercialized due to the many challenges related to their Li anodes, cathodes and electrolytes, and the interfaces among these components.[12] Among the issues of LMBs, their interfacial stability is of particular importance and certainly needs some special attention.

The direct contact between an Li anode (or a cathode) and a liquid electrolyte is prone to cause some undesirable reactions. Parasitic reactions produce a passive layer on the Li anode (or on the cathode), which is called solid electrolyte interphase (SEI) (or cathode electrolyte interphase (CEI)).[12,13] CEI was only coined recently to distinguish it from SEI. Regardless, in many studies, people often conflate CEI with SEI. Both SEI and CEI are products of decomposed electrolytes and cyclable Li, but they differ in their composition. In addition, the composition and properties of either an SEI or a CEI also vary with electrolytes and the operational conditions used. It is very important to maintain their stability to prevent the continuous formation of SEI and CEI. Unfortunately, naturally formed SEI and CEI are often unstable.[13] On the anode side, the volume expansion and contraction of Li anodes due to plating and stripping, respectively, cause cracking of SEI, exposing fresh Li to interact with the electrolyte that results in continuous formation of the SEI. As a consequence, LMB cells are prone to exhibiting an ever-increasing overpotential and low Coulombic efficiency (CE). An unsteady CEI, such as that in the case of metal oxide cathodes, is vulnerable to hydrofluoric attacks, microcracking, irreversible phase transition, and transition metal dissolution. All these issues lead to fading performance and eventually cell failure. Many strategies have been adopted to address these issues related to Li anodes and different cathodes, such as adding additives to electrolytes, doping elements to cathodes, and surface coatings for Li anodes and cathodes.[14,15] Among them, surface coating is a facile and effective strategy for protecting both Li anodes and LMB cathodes from degradation, which has been practiced *via* various techniques, including chemical vapor deposition (CVD), physical vapor deposition (PVD), and wet chemistry. PVD is limited due to the material choice and its line-of-sight deposition nature, while CVD typically needs high temperatures ($>$500 °C).[16,17] Additionally, wet chemistry is not feasible for the use of air-sensitive materials as coatings. Considering the low melting point of Li anodes ($\sim$180 °C), a coating technique applicable at low process temperatures is desired.

Compared to traditional coating techniques, recently two unique methods emerged and showed powerful capabilities for coating Li anodes and various cathodes, *i.e.*, atomic and molecular layer deposition (ALD and MLD). Particularly, they feature precise material growth and enable conformal and uniform thin film coatings at the atomic/molecular level. Also, they are feasible for application on almost any substrate due to their surface-controlled nature and low process temperatures that can be as low as even room temperature.[18] They share the same working principle but target inorganic and organic materials, respectively, through adopting different precursors. Since the 2010s, ALD and MLD have been recognized as two powerful tools for addressing interfacial issues of LIBs and beyond.[18] Recently, Meng comprehensively reviewed the developments in ALD and MLD for rechargeable batteries.[19] They have been used to develop a large variety of coating materials for tackling various battery issues.

In this Feature Article, we aim to introduce our recent exciting progress on LMBs and showcase the novel surface coatings we have developed *via* ALD and MLD. Particularly, we highlight our achievements in developing Li‖NMC LMBs, where NMCs are Ni-rich ($x \geq 0.6$), such as $LiNi_{0.6}Mn_{0.2}Co_{0.2}O_2$ (NMC622) and $LiNi_{0.8}Mn_{0.1}Co_{0.1}O_2$ (NMC811). To modify NMC cathodes, we have investigated various coatings obtained *via* ALD, including binary oxides, Li-containing oxides, and sulfides. Very encouragingly, our discovery of sulfide coatings

Xiangbo Meng

Dr Xiangbo Meng is an Associate Professor of Mechanical Engineering at the University of Arkansas, USA. He holds two PhD degrees: one in Mechanical & Materials Engineering (2011) and another in Chemical & Biochemical Engineering (2008), both from the University of Western Ontario, Canada. He conducted postdoctoral research at Argonne and Brookhaven National Laboratories in the U.S. from 2011 to 2016. Since he joined the University of Arkansas in 2016, he has led a research group focused on advancing battery technology, with a particular emphasis on using atomic and molecular layer deposition (ALD and MLD) for interface modification.

represents a breakthrough that has some special benefits for NMC cathodes. On the Li anodes, we have developed several novel Li-containing polymeric coatings *via* MLD. Significantly, we demonstrated that our ALD-resultant inorganic coatings and MLD-resultant polymeric coatings could work synergistically in Li‖NMC cells to maximize cell performance. Thus, this Feature Article is expected to inspire peer researchers to better utilize ALD and MLD to develop advanced rechargeable batteries, such as LMBs, solid-state batteries (SSBs), and other alkali metal batteries.

2. Principles of ALD and MLD

Both ALD and MLD are based on surface-controlled chemistry, which helps film growth proceed in a precise manner and contributes to unrivaled film uniformity and conformality. Fig. 1a illustrates an ALD process for growing zirconium oxide (ZrO_2) using tetrakis(dimethylamido)zirconium(IV) ($Zr(NMe_2)_4$ or TDMA-Zr) and H_2O,[20,21] whose growth mechanism is based on ligand exchange of –OH and $–NMe_2$ (Me = CH_3). Using this ALD process, Liu *et al.* deposited ZrO_2 thin films onto graphene nanosheets (GNS)[22] and nitrogen-doped carbon nanotubes (N-CNTs).[23] They explained the growth mechanism with two consecutive surface reactions that are expressed as follows:

$$|–OH + Zr(NMe_2)_4\ (g) \rightarrow |–O–Zr(NMe_2)_3 + HNMe_2\ (g) \quad (1)$$

$$|–O–Zr(NMe_2)_3 + 3H_2O\ (g) \rightarrow |–O–Zr(OH)_3 + 3HNMe_2\ (g) \quad (2)$$

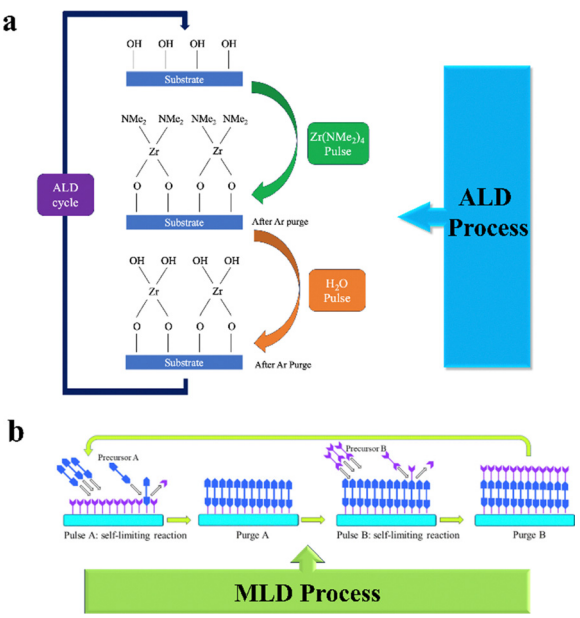

Fig. 1 (a) Schematic illustration of the ALD deposition of zirconium oxide (ZrO_2) using TDMA-Zr and H_2O as precursors. Adapted with permission from ref. 21. Copyright 2020, Materials Research Society. (b) Schematic illustration of a general MLD process using two homobifunctional organic precursors of A and B. Adapted with permission from ref. 18. Copyright 2024, Inorganic Chemistry Frontier.

where "|–" indicates the surface species and "(g)" denotes the gas phase species. These two surface reactions lead to the growth of ZrO_2 and are repeated to grow ZrO_2 into thicker films in a controllable layer-by-layer manner. A complete ALD cycle, encompassing the four steps outlined in Fig. 1a, involves a sequence of pulsing TDMA-Zr, purging the overdose of TDMA-Zr and byproducts, pulsing H_2O, and finally purging the overdosed H_2O and byproducts. By increasing the cycle number, the ZrO_2 film can grow into any desired thickness.

By adopting long-chain organic precursors, the MLD could also proceed to deposit organic materials in a layer-by-layer mode at the molecular level. Fig. 1b illustrates a general MLD process for growing pure polymers by adopting two homobifunctional precursors. First, the precursor A molecules are dosed, which incur a reaction with the reactive sites on the substrate surface through a specific linking chemistry, resulting in the addition of a molecular layer that introduces new reactive sites onto the substrate surface. After A is thoroughly purged, the precursor B molecules are dosed to interact with the newly formed reactive sites, generating another molecular layer and restoring the surface to its original reactive groups. Subsequently, purging of B is conducted to complete one MLD cycle (Fig. 1b). By repeating the aforementioned steps, the MLD accurately grows polymeric films to a desirable thickness.

To date, a large variety of organic and inorganic coatings obtained *via* ALD and MLD have been investigated to overcome various interfacial issues related to the cathode and anode interfaces. In the following parts, we will give an overview of the coatings related to Li‖NMC cells and highlight the novel coatings from our recent studies.

3. Li anode interface

To develop advanced battery technologies, researchers have explored and employed alternative anode materials other than commercial graphite to boost the energy density.[9,24–26] Among potential candidates, alkaline metals are very promising, including Li,[9,27] sodium (Na),[28,29] and potassium (K),[30,31] with specific capacities that are higher than that of the graphite anode ($\sim$372 mA h g^{-1}), *i.e.*, $\sim$3860, $\sim$1166, and $\sim$685 mA h g^{-1}, respectively. Among them, the Li metal has widely gained recognition as an ideal candidate due to its ultrahigh theoretical capacity of $\sim$3860 mA h g^{-1} and very low redox potential of −3.040 V *vs.* SHE. However, two daunting challenges must be addressed before Li anodes can be commercially practiced in rechargeable LMBs. First, the Li dendritic growth during plating poses serious safety risks.[32,33] Second, the SEI can form continuously once the fresh Li surfaces are exposed to the electrolyte. While forming the SEI, spontaneous reactions between the Li metal and the electrolyte cause the Li metal anode to undergo significant volumetric and morphological changes with repeated plating/stripping.[34,35] This ionically conductive, but electronically insulating SEI layer, can thicken and become porous with increased cycles.[36–38] At the same time, the SEI not only consumes Li and electrolytes, but also

has increased internal impedance, which diminishes the battery's cycling life.[24,39] Notably, the continuous growth of the SEI and dendrites during the repetitive plating and stripping processes poses a critical risk because the Li dendrites can go through the cell's separator, reach the cathode side, and cause internal short circuits that eventually lead to fire and explosion.

Given the substantial safety concerns arising from the uncontrollable interface reactions between the Li metal and electrolyte, these issues must be urgently addressed.[40–42] Several strategies have been used in the past, such as the development of three-dimensional (3D) hosts to control and regulate the expansion of Li,[18,43,44] electrolyte designs to minimize side reactions,[15,31] and surface coating of Li anodes.[45–50] Among them, the approach of surface coating has been proven to be facile and effective. To this end, our recent studies have developed several novel Li-conducting coatings, *i.e.*, $L_{ix}Al_yS$ (LAS)[51] *via* ALD and lithicones (LiGL (GL = glycerol), LiTEA (TEA = triethanolamine), and LiHQ (HQ = hydroquinone)) *via* MLD.[1,52–54] All these Li-containing coatings have demonstrated exceptional protective effects on the Li anodes, and they have remarkably extended the cyclability of Li‖Cu asymmetric cells, Li‖Li symmetric cells, and Li‖NMC full cells, as discussed in detail below.

3.1 ALD coatings over the Li anodes

The first ALD attempt to protect Li anodes was reported with an Al_2O_3 coating,[49,50] followed by TiO_2,[55] ZrO_2.[56] Later, the Li-containing coatings, such as Li_3PO_4[57] and LAS,[51] were studied for improved ionic conductivity. These ALD coatings are typically thin and uniform, *i.e.*, less than 15 nm. These studies demonstrated that surface coating *via* ALD can effectively enhance the cycling life of Li‖Li symmetric cells, Li‖Cu asymmetric cells, and Li‖cathode LMB full cells. All these surface coatings have been investigated to determine their ability to inhibit the formation of lithium dendrites over a specific number of Li-stripping/plating cycles. Some studies have also revealed that the homogeneity of the interfacial layer is important. A uniform and thin interfacial layer can regulate ion flux and minimize interfacial impedance. It not only reduces internal impedance, but also preserves the energy density of the cell.[58,59] During the Li-stripping/plating processes, the aforementioned thin ALD coatings might slowly evolve and degrade. For example, Al_2O_3 and TiO_2 have been proposed to convert into $Li_xAl_2O_3$[60,61] and $Li_2Ti_2O_4$,[62,63] respectively. Therefore, the gradual process of evolution of these coating layers may limit the lifespan of Li anodes. In our studies, we have developed a new ALD growth for Li anodes, *i.e.*, LAS and also confirmed that the LAS coating could stabilize the interface of Li‖Li symmetric cells, significantly decrease the formation of the SEI, and minimize the impedance of the cells. We also found that, in comparison to the pronounced lithium dendrites that formed on bare Cu foils, applying a 50-nm-thick LAS coating onto the copper foil could prevent the formation of lithium dendrites during plating. The LAS coating allows a relatively higher ionic conductivity of 2.5×10^{-7} S cm^{-1} at room temperature. Despite these efforts, ALD coatings to date are usually undesirable for tackling the issues typically associated with Li anodes and could only be coated very thin due to their non-ideal properties. To this end, our recent efforts to achieve flexible Li-containing polymeric coatings *via* MLD are very encouraging, as discussed in the following section.

3.2 MLD coatings over Li anodes

The first practice of MLD on Li anodes was unveiled in 2018. To date, only a few polymeric MLD coatings have been reported in the literature, such as polyurea,[64] AlEG (*e.g.*, EG = ethylene glycol),[65,66] and ZrEG.[67] These polymer coatings are more flexible compared to inorganic films obtained by ALD, but their ionic conductivity is questionable. To develop ionically conductive polymeric films *via* MLD, we have recently been focusing on studying Li-containing polymers. To date, we have reported LiGL,[1] LiTEA,[54] and LiHQ,[53] which are polymeric lithium alkoxides with carbon-containing backbones, *i.e.*, –Li–O–R–O–Li–. Commonly, they are named as lithicones.

3.2.1 LiGL. By utilizing GL and lithium *tert*-butoxide (LTB) as precursors, our group first developed a new MLD process to grow the LiGL lithicone at 150 °C (Fig. 2a-i). The growth of LiGL was monitored using an *in situ* quartz crystal microbalance (QCM) to acquire time-resolved mass changes in ng cm^{-2} (Fig. 2a-ii–iv). To establish a repeatable and uniform starting surface, an Al_2O_3 film was pre-deposited on the QCM crystal using ALD (inset of Fig. 2a-ii). In this study, the unit structure of LiGL has been suggested to be $(CH_2CHCH_2)(OLi)_3$, which has been verified by XPS (X-ray photoelectron spectroscopy) analysis. The overall reaction between GL and LTB is assumed to be as follows (expression (3)):

$$3LiO^tBu + (CH_2CHCH_2)(OH)_3 \rightarrow (CH_2CHCH_2)(OLi)_3 + 3HO^tBu \quad (3)$$

After applying the MLD-resultant LiGL onto Li anodes, we investigated its protection effects. The deposited LiGL coatings were varied in their thicknesses by adjusting the cycles of LiGL coating with MLD and were differentiated as LiGL-*X* (where *X* represents the number of MLD cycles). LiGL-0 denotes the bare Li electrode. The LiGL-coated and uncoated Li electrodes were assembled in Li‖Li cells and tested at two current densities of 2 and 5 mA cm^{-2} under a fixed areal capacity of 1 mA h cm^{-2} using an ether electrolyte. The electrolyte was 1 M lithium bis(trifluoromethanesulfonyl)imide (LiTFSI) in a 1 : 1 volume ratio of 1,3-dioxolane (DOL) and 1,2-dimethoxyethane (DME). The results demonstrated that the LiGL coatings enabled exceptional protection over the Li anodes and greatly extended the cyclability of the Li‖Li cells (Fig. 2b and c). Particularly, it was found that, in terms of cell overpotential, a thicker LiGL coating performed better. Among the LiGL coatings obtained *via* the different MLD cycles, the coating thickness could go up to ~250 nm (LiGL-90), while the lowest cell overpotential was achieved at 2 mA cm^{-2} (Fig. 2b). Similarly, LiGL-60 is the thickest coating investigated at 5 mA cm^{-2} that exhibited the best performance (Fig. 2c). The LiGL-coated Li‖Li cells did not fail after 5500 and 5200 hours, when they were tested at 2 and 5 mA cm^{-2},

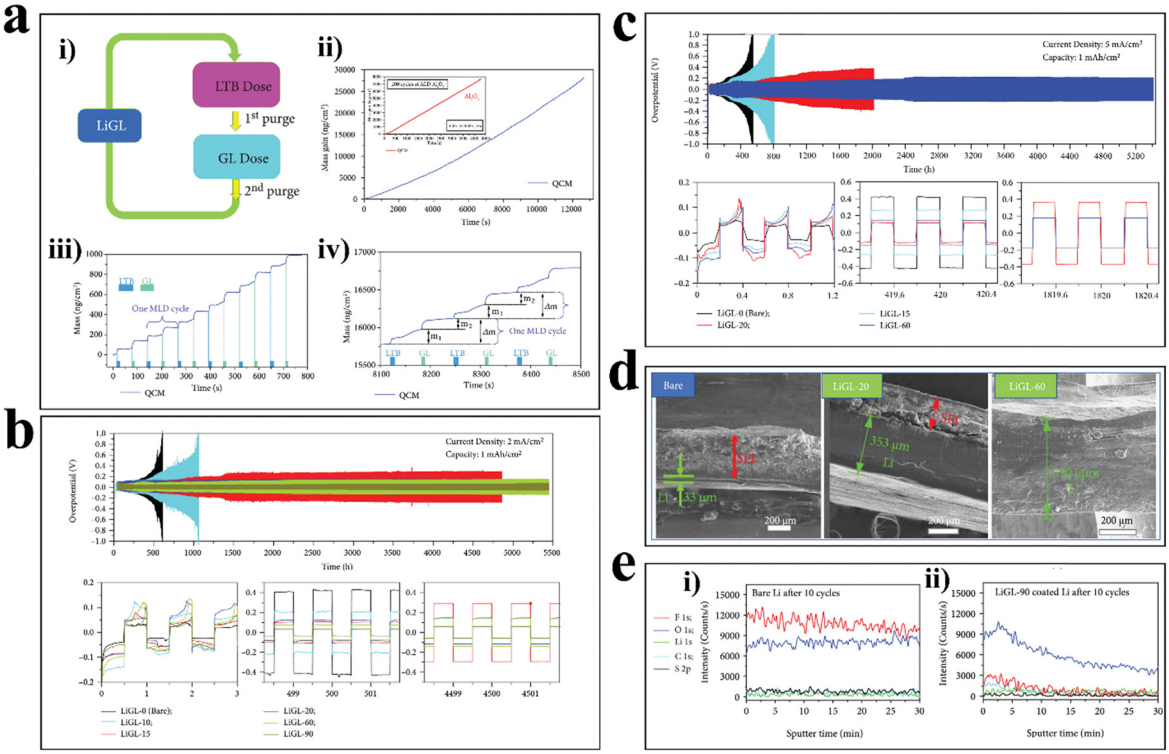

Fig. 2 (a) Growth step for MLD LiGL lithicone: (i) scheme for LiGL MLD process. (ii) QCM measurements at 150 °C for 100 cycles (inset: ALD–Al_2O_3 QCM growth of 200 cycles before MLD LiGL). (iii) QCM profile during the initiation region (first 10 cycles), (iv) QCM profile in a stable growth region. Effect of Li coatings on Li-metal anodes at different current densities: (b) 2 and (c) 5 mA cm^{-2}, keeping the fixed areal capacity of 1 mA h cm^{-2}. (d) SEM images of the cross-sections of the Li electrodes after 700 Li-stripping/plating cycles. (e) XPS depth profiling of (i) bare Li and (ii) LiGL-90 electrodes after 10 Li-stripping/plating cycles. Adapted with permission from ref. 1. Copyright 2021, Energy Material Advances.

respectively. In this work, we did not further minimize the cell overpotential to optimize the coating thickness. Regardless, these results implied that the LiGL coatings are excellent ion conductors. This was verified in one of our follow-up studies[52] in which an ionic conductivity of $\sim 10^{-4}$ S cm^{-1} was revealed for LiGL at room temperature, while LiGL-400 ($\sim$1 μm) still worked and featured the best safety.

Using scanning electron microscopy (SEM), we further examined the change in the morphology of bare and LiGL-coated Li electrodes after cycling to have a better understanding of the protective effects of the LiGL coating. It was found that all the LiGL coatings more or less protected Li electrodes from corrosion, but the LiGL-60 coating could completely depress Li plating from dendritic growth, thus avoiding the formation of SEI in 700 Li-stripping/plating cycles (Fig. 2d). These results are consistent with the electrochemical cycling performance in Fig. 2b and c. XPS analyses on cycled bare (Fig. 2e-i) and LiGL-90 electrodes (Fig. 2e-ii) further verified that based on the evolution of fluorine (F), along with the film depth, a thick LiGL coating (*e.g.*, LiGL-90) could effectively suppress the formation of the SEI. Specifically, the F signal of the bare Li electrode after 10 Li-stripping/plating cycles (Fig. 2e-i) was very strong, but it did not fade with film depth. F is regarded as a component of the SEI that forms from the decomposition of the LiTFSI salt in the ether electrolyte. Inorganic fluorides, such as LiF, can enhance interfacial stability, but they have very low ionic conductivity ($\sim 10^{-10}$ S cm^{-1}). Thus, a thick LiF layer could slow ion conduction and increase cell impedance and overpotential.[68,69] This is consistent with the quick increase in cell overpotential of bare Li‖Li cells in Fig. 2b and c. In contrast, the F signal of the cycled LiGL-90 electrode (Fig. 2e-ii) was very weak, and it faded quickly along the film depth, implying much less SEI formation or some diffusion of F in the top layer of the LiGL coating. These results again verified that the LiGL coatings protected Li from SEI formation and interfacial degradation.

Our recent study[52] further corroborated that a thick LiGL is favorable to protect Li electrodes, and coating thickness could go up to 400 MLD cycles or $\sim$1080 nm (Fig. 3). Such a thick coating has never been reported previously, and it was demonstrated to be workable as a surface coating *via* MLD. In this study, we were also able to disclose that the LiGL coating is highly conductive ionically and enables an ionic conductivity of $\sim 10^{-4}$ S cm^{-1} at room temperature. Such an excellent ion conduction by the LiGL coating underlies its workability under a large thickness. Using a local high-concentration electrolyte (LHCE) composed of lithium bis(fluorosulfonyl)imide (LiFSI), 1,2-dimethoxyethane (DME), and 1,1,2,2-tetrafluoroethyl-2,2,3,3-tetrafluoropropyl ether (TTE) in a molar ratio of 1 : 1.2 : 3, in the study, we particularly demonstrated that the LiGL coatings could remarkably improve the LMBs of Li‖NMC622 ($LiNi_{0.6}Mn_{0.2}Co_{0.2}O_2$) (Fig. 3a–d).

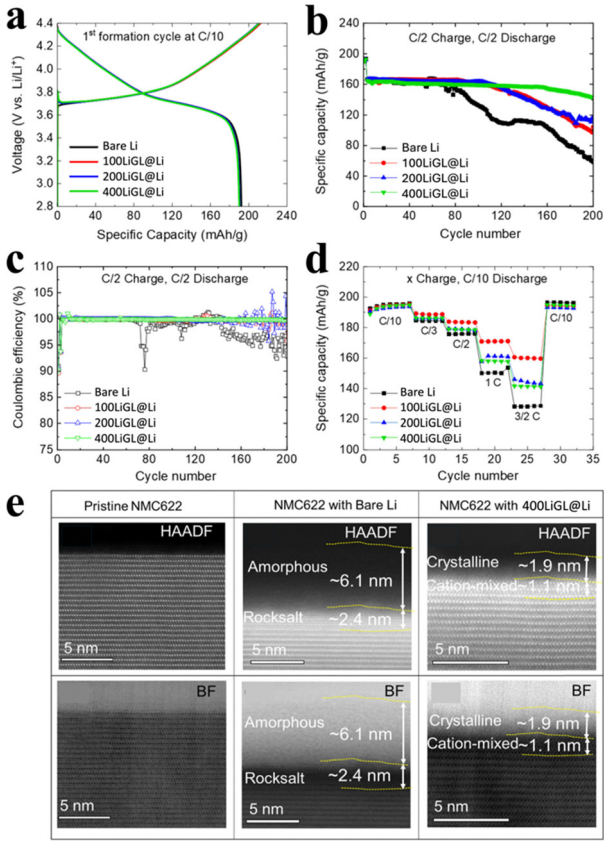

Fig. 3 The effects of LiGL-coated Li anodes on Li‖NMC622 cells. (a) The first charge/discharge profiles of full cells with bare Li and LiGL-coated-Li coupled with NMC622 (1C = 4.2 mA cm^{-2}). For different thicknesses of the Li coating at 2.8–4.4 V, (b) cyclability at C/2, (c) CE at C/2, (d) C-rate, and (e) HAADF and BF images of pristine NMC622 coupled with coated and uncoated Li. Adapted with permission from ref. 52. Copyright 2024, Small Structures.

The Li‖NMC622 cells were first tested with two formation cycles at a C/10 rate (1C = 4.2 mA cm^{-2}), followed by a C/2 rate testing for charge and discharge cycles within a voltage window of 2.8–4.4 V. The three full cells with the LiGL-coated Li anodes improved significantly in terms of cycling stability, upon being cycled at a C/2 rate. Very interestingly, the full cells exhibited longer cycling life and higher capacity retention with a thicker LiGL coating on the Li metal (*i.e.*, LiGL 400). High-angle annular dark-field (HAADF) and bright field (BF) transmission electron microscopy (TEM) analysis revealed that after 200 charge–discharge cycles, the NMC622 cathode coupled with the bare Li exhibited a thicker CEI layer and the formation of a rocksalt phase on the electrode's surface. In contrast, the NMC622 cathode, coupled with an LiGL400-coated Li only showed a very thin layer of CEI and cation mixed surface (Fig. 3e). This means that the LiGL MLD coating cannot only suppress dendrite and SEI formation on the anode side, but also helps suppress the composition and structure of the interfaces on the cathode surface. This is attributed to the reduced crosstalk from the LiGL-coated Li anode to the NMC622 cathode, which suppresses the side reactions between the NMC622 particles and radicals.[70] In addition, the improvement in the cycling life of the full cells can also be attributed to the thin and uniform CEI layer formed at the surface of the cathode owing to the adoption of the LiGL-coated Li anodes. It has been shown that CEI is very important to ensure the good structural stability of the NMC cathodes.[71]

Considering all these factors together, we ascribed the superior protection of the LiGL coatings over the Li anodes to their exceptional properties, such as excellent ionic conductivity, electronically insulating nature, mechanical flexibility, chemical stability, and chemical compatibility. However, we observed some cracks over the LiGL coatings after cell assembly, suggesting that the mechanical strength of the LiGL coatings should be further improved.

3.2.2 LiTEA. The remarkable effects of LiGL on Li anodes inspired us to develop new lithicones *via* MLD. Given the moderate mechanical strength of LiGL, we adopted a new precursor, TEA (*i.e.*, $N(CH_2CH_2OH)_3$), for coupling with LTB to grow a new lithicone, LiTEA. The TEA precursor has a larger molecular weight. Therefore, we expected that LiTEA would enable some improvement in mechanical properties.

Similar to the study on LiGL, we first studied the growth of LiTEA on a repeatable ALD-deposited Al_2O_3 surface using the *in situ* QCM, which exhibited a linear relation with increased MLD cycles.[54] Using SEM, we further revealed that the mean GPC of the MLD LiTEA is ~3.6 Å $cycle^{-1}$ and verified its composition using XPS. The underlying growth mechanism was suggested using the following eqn (4):

$$3LiO^tBu + N(CH_2CH_2OH)_3 \rightarrow N(CH_2CH_2OLi)_3 + 3HO^tBu \quad (4)$$

We applied the resultant LiTEA with adjustable MLD cycles on Li chips to investigate its protective effects in Li‖Li cells. The LiTEA-coated Li chips were then named LiTEA-*X*, where *X* stands for the number of MLD cycles (*e.g.*, *X* = 0, 40, 80, 100 200, 300, 400, and 500 MLD cycles). As illustrated in Fig. 4, the LiTEA coatings could stabilize the cell overpotential, while LiTEA-200 electrodes enabled the lowest cell overpotentials under two different current densities (2 and 5 mA cm^{-2}), implying that the coating thickness of LiTEA-200 (~72 nm) was optimal for protecting Li electrodes. In other words, a thinner LiTEA coating may not adequately protect Li electrodes from degradation, while a thicker LiTEA coating may impede Li^+ ions from transport. From Fig. 4, it is concluded that the LiTEA coatings helped Li‖Li cells achieve long-term cyclability, while the bare Li‖Li cells failed quickly with dramatically increased cell overpotentials. To this end, LiTEA coatings must be at least from 80 MLD cycles.

Observation of the cycled Li electrodes (after 500 Li-stripping/plating cycles at 2 mA cm^{-2} and 1 mA h cm^{-2}) using SEM (Fig. 4c) allowed us to further verify that an LiTEA coating thicker than 80 MLD cycles could better protect Li electrodes from corrosion, while the LiTEA-200 electrodes showed no evident degradation, judging from the surface morphology and cross-section. In terms of surface appearance (Fig. 4c, top),

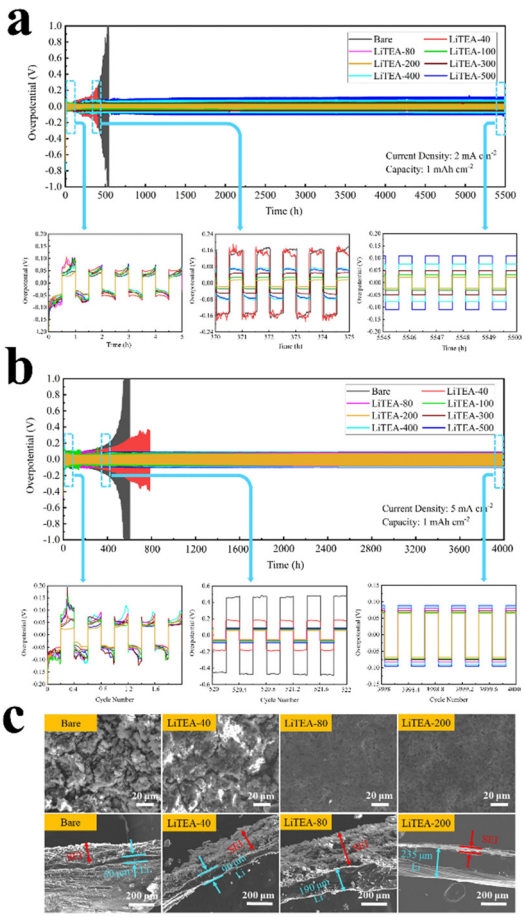

Fig. 4 The effect of LiTEA-coating on Li-metal electrodes at different current densities (a) 2 and (b) 5 mA cm^{-2} at a fixed areal capacity of 1 mA h cm^{-2}. (c) The SEM images of Li electrode surfaces (top images) and electrode cross-sections (bottom images) for bare and coated Li electrodes after 500 Li-stripping/plating cycles at 2 mA cm^{-2} and 1 mA h cm^{-2}. Adapted with permission from ref. 54. Copyright 2023, Chemical Engineering Journal.

first, the LiTEA-80 and LiTEA-200 exhibited much denser and smoother surfaces than those of LiTEA-40 and LiTEA-0. The remarkably porous surface structures of LiTEA-0 and LiTEA-40 are due to the formation of the SEI. Second, the cross-sectional characteristics of Li electrodes (Fig. 4c, bottom) revealed that there was less and less SEI formation with increased thickness of the LiTEA coating from LiTEA-40 to LiTEA-80 and LiTEA-200. Impressively, the LiTEA-200 cross-section appeared to be nearly intact with minimal formation of the SEI; the Li layer thickness was almost unchanged after 500 Li-stripping/plating cycles (Fig. 4c).

All these results demonstrated that the LiTEA MLD coating exhibited exceptional protective effects on the Li electrodes. It could remarkably suppress the formation of the SEI and inhibit Li dendrites from forming as well. We believe that these benefits are due to the excellent properties of the LiTEA coating, including effective electric insulation and ionic conduction, as well as chemical and electrochemical stability.

3.2.3 LiHQ. Different from the cross-linked LiGL and LiTEA, recently we also developed a new lithicone of LiHQ *via* MLD and investigated its protective effects on the Li electrodes in the Li‖Li symmetrical cells and Li‖NMC811 full cells. Due to its aromatic backbone, LiHQ is expected to provide structural stability.

In the study, we revealed that the MLD of LiHQ was a feasible process with an average GPC of ~4 Å $cycle^{-1}$.[53] Furthermore, we also demonstrated that in the Li‖Li cells, the LiHQ coating could effectively protect Li electrodes from degradation with a sufficient coating thickness of ≥75 MLD cycles (~20 nm). As shown in Fig. 5a and b, LiHQ-75 performed the best, in terms of cell overpotential and cyclability. Furthermore, SEM observations (Fig. 5c) confirmed that after 200 Li-stripping/plating cycles at 2 mA cm^{-2} and 1 mA h cm^{-2}, the LiHQ-75 could protect Li effectively from degradation, while LiHQ-50 mitigated Li corrosion and bare Li degraded severely. Particularly, our XPS analysis (Fig. 5d) revealed that for bare Li‖Li cells, the ether electrolyte experienced significant reduction during the electrochemical cycling, leading to the formation of an SEI layer composed of organic compounds (*e.g.*, $C_2H_4OCH_2CH_2$) and inorganic compounds (*e.g.*, LiF, Li_2CO_3, Li_2O, and Li_3N). In contrast, the LiHQ-75 coating remarkably protected the electrolyte from decomposition. This was confirmed by XPS analysis and the cycled LiHQ-75 had much less degraded by-products (*e.g.*, LiF and Li_2CO_3).

4. Cathode interface

Creating a uniform shell around the active particles of cathode materials is crucial for stabilizing the cathode/electrolyte interface. This shell serves as a protective layer and minimizes the possibility of parasitic reactions. Additionally, precise control over the thickness of the nanoscale coating is vital for effective charge transfer, particularly considering the limited Li^+ transportation capability of inert coating materials. In the past decade, the ALD technique has emerged as a vapor-phase alternative to wet chemical methods. This method offers distinct advantages in producing high-quality, conformal, and uniform films, regardless of whether it is applied to electrode powders or prefabricated electrodes.[72,73] Particularly, Ni-rich NMCs ($X \geq 0.6$) have attracted significant attention, primarily due to their cost-effectiveness and high capacity. To date, a variety of coatings have been documented for the modification of Ni-rich NMCs using wet chemistry and ALD, including oxides (*e.g.*, Al_2O_3,[74,75] TiO_2,[76] WO_3,[77] Co_3O_4,[78] ZrO_2,[79] and ZnO[80]), lithium metal oxides (*e.g.*, $LiNbO_3$,[81] Li_2ZrO_3,[82,83] $LiAlO_2$,[84,85] $Li_4Ti_5O_{12}$,[86] and $LiAlF_4$[87]), phosphates,[88] fluorides,[89,90] and sulfides.[91] Among these coatings, our recent discoveries about Li-containing coatings and sulfides are especially significant, and thus, they will be discussed in detail and highlighted in the following parts.

4.1 ALD coatings of metal oxides

4.1.1 TiO_2. Among transition metal oxides, TiO_2 has been studied as a coating due to its unique properties, such as low cost, abundance in nature, non-toxicity, and chemical stability. ALD features tremendous capabilities, including varying GPC,

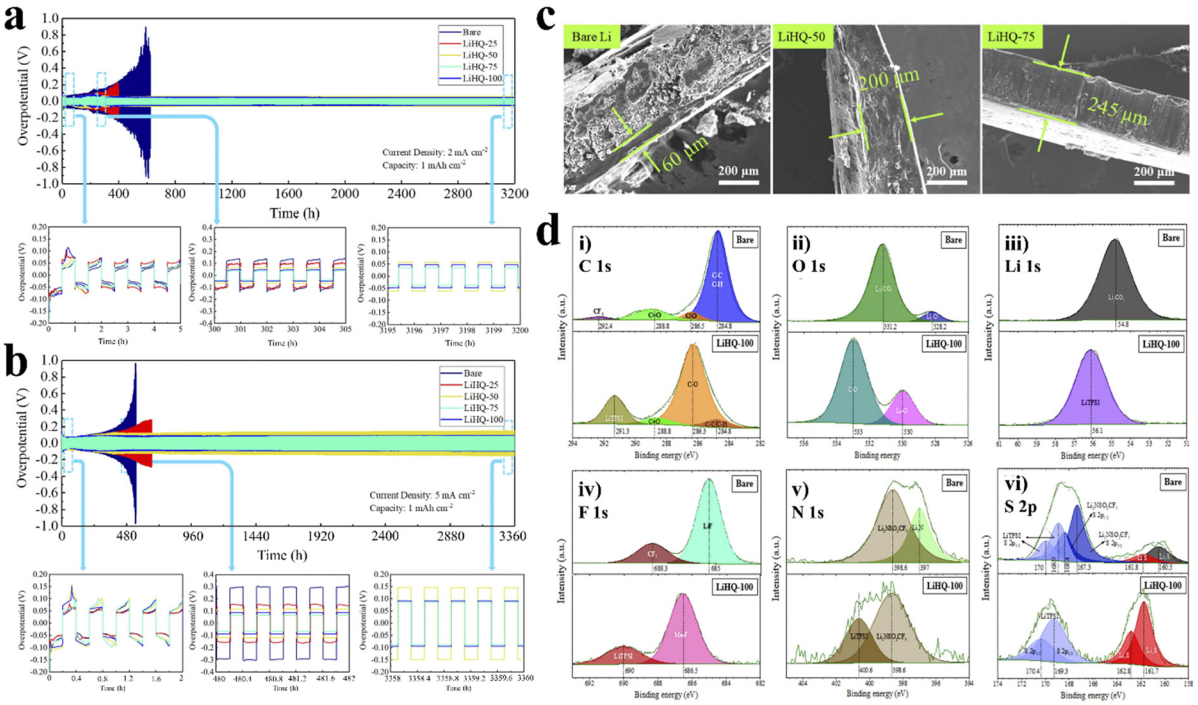

Fig. 5 The protective effects of the LiHQ coating on the Li||Li symmetrical cells. Electrochemical cyclability of the Li||Li cells at different current densities (a) 2 and (b) 5 mA cm^{-2} at a fixed areal capacity of 1 mA h cm^{-2}. (c) SEM images of the cross sections of cycled Li electrodes, including bare Li, LiHQ-50, and LiHQ-75 electrodes after 200 Li-stripping/plating cycles. (d) High resolution XPS spectra of (i) C 1s, (ii) O 1s, (iii) Li 1s, (iv) F 1s, (v) N 1s, and (vi) S 2p after 10 Li-striping/plating cycles in an ether electrolyte; these tests were performed at a current density of 2 mA cm^{-2} and a fixed areal capacity of 1 mA h cm^{-2} for bare Li and LiHQ-75-coated Li. Adapted with permission from ref. 51. Copyright 2024, Nano Energy.

crystallinity, and morphology of the resultant films, by adopting different precursors, growth temperatures, and substrates.[92–94] Previously, ALD was utilized to develop various nanostructures with TiO_2, such as 0D composite TiO_2 nanoparticles,[95,96] 1D nanotubes,[97] 2D planar films,[98,99] and other complicated nanostructures.[93,100] In addition, a variety of precursors[92–94] were used to develop ALD–TiO_2; titanium tetra-isopropoxide (TTIP, $Ti(OCH(CH_3)_2)_4$) and deionized water are the most commonly used pair as titanium and oxygen sources, respectively. Utilizing TTIP and H_2O, we deposited TiO_2 *via* ALD over three different substrates, *i.e.*, commercial porous anodic aluminum oxide (AAO) templates, multi-walled carbon nanotubes (MWCNTs), and graphene nanosheets (GNSs).[92] As a result, three different nanostructures were produced, *i.e.*, pure TiO_2 nanotubes (Fig. 6a-i and ii), CNT–TiO_2 coaxial tubular hybrids (Fig. 6a-iii and iv), and GNS (Fig. 6a-v)-supported TiO_2 (Fig. 6a-vi). Two growth temperatures had been applied, *i.e.*, 150 and 250 °C. The former led to amorphous TiO_2, while the latter resulted in crystalline TiO_2. The average GPC of ALD–TiO_2 at 150 °C is ~0.29 and ~0.34 Å $cycle^{-1}$ for CNTs and AAO, respectively. It increased to ~0.40 and ~0.71 Å $cycle^{-1}$ at 250 °C for CNTs and AAO, respectively. The higher density of reactive sites in AAO compared to CNTs is most likely the cause of the higher growth in AAO than in CNTs. In the case of GNS, the GPC can be calculated with the help of the following formula.

$$\text{GPC} = (\text{thickness of the coated wrinkles} - \text{thickness of pristine wrinkles})/(2 \times \text{number of cycles})$$

In Fig. 6a-vi, the GPC is ~0.19 Å $cycle^{-1}$ (the average GNS wrinkle thickness is ~3.4 nm). The apparent changes in the thickness of all the substrates confirm the successful completion of the ALD of TiO_2 coating (Fig. 6a-i–vi).

We have also examined ALD–TiO_2[76] on the prefabricated NMC 622 electrode to mitigate the parental defects[12] associated with the Ni-rich NMCs at high voltage. We achieved different ALD–TiO_2 thicknesses (20, 40, 60, and 100 ALD cycles) at 120 °C, referred to as ALD–TiO_2-*X*, where *X* is the number of TiO_2 ALD cycles. XPS and X-ray fluorescence (XRF) validate the surface chemistry and homogeneity of the ALD–TiO_2 coating. To validate our hypothesis of minimizing the parasitic reactions on the NMC surfaces, the optimal coating of the ALD–TiO_2-coated NMC 622 sample (ALD–TiO_2-20), along with the uncoated sample (ALD–TiO_2-0), was tested in the half-cell configuration with Li metal as an anode (Fig. 6b-i) within two different voltage windows of 2.8–4.4 and 2.8–4.5 V. The full cell was tested with graphite as an anode in the range of 2.8–4.45 V under C/3 (Fig. 6b-ii). One could easily observe that both the half and full cells improved remarkably in their sustainable capacity and capacity retention. The underlying mechanism lay in the protective roles played by the ALD–TiO_2 coating, such as: (1) strengthening the mechanical integrity of the NMC electrodes; (2) mitigating the oxidation of the electrolyte solvent; (3) decreasing the degree of cation mixing of the NMC electrodes; and (4) reducing the dissolution of transition metals. All these benefits are interconnected. As shown in Fig. 6b-iii and iv, the ALD–TiO_2-20 effectively protected the NMC electrode from

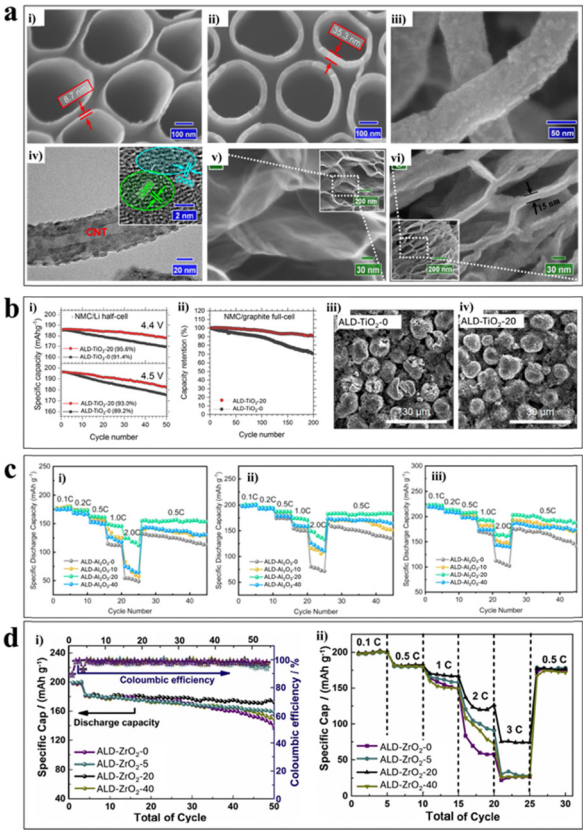

Fig. 6 (a) Template-guided ALD–TiO_2 at 250 °C. The SEM micrograph depicting AAO templates coated with (i) 200 and (ii) 500 cycles of ALD–TiO_2. ALD–TiO_2 deposited on CNTs at 250 °C. (iii) 100 cycles of ALD–TiO_2 and TEM Images displaying (iv) 100 cycles of ALD–TiO_2. Adapted with permission from ref. 92. Copyright 2023, Applied Surface Science. SEM images of (v) GNSs and (vi) 300 cycles of TiO_2-GNSs. Adapted with permission from ref. 93. Copyright 2011, Nanotechnology. (b) For ALD–TiO_2-0 (bare NMC), and ALD–TiO_2-20 (ZrO_2 coated NMC) (i) cyclability in half-cell configuration within two different voltage windows of 2.8–4.4 V or 2.8–4.5 V *vs.* Li/Li^+ under a 0.1C current density. (ii) Full cell configuration within the voltage window of 2.8–4.45 V *vs.* graphite under a 0.33C current density. FIB-SEM micrographs of (iii) ALD–TiO_2-0 electrode and (iv) ALD–TiO_2-20 electrode after 45 cycles at a current of 0.5C within the voltage range of 3.0–4.5 V. Adapted with permission from ref. 69. Copyright 2019, Chemistry of Materials. (c) Rate capability of ALD–Al_2O_3-*X*, (where *X* = 0, 10, 20, and 40 number of Al_2O_3 ALD cycles) at different current densities within the voltage ranges of (i) 3.0–4.3 V, (ii) 3.0–4.5 V, and (iii) 3.0–4.7 V. Adapted with permission from ref. 101. Copyright 2020, Nanotechnology. (d) Electrochemical activity of NMC622-*X* ZrO_2 (where *X* = 0, 5 20, and 40 number of ZrO_2 ALD cycles) within voltage window 3.0–4.5 V, (i) cyclability at 0.5C rate, (ii) C-rate testing. Adapted with permission from ref. 79. Copyright 2020, Journal of Material Science and Technology.

cracking, which was recovered from the cycled full cells (Fig. 6b-iv). In contrast, the ALD–TiO_2-0 electrode suffered from severe cracking. Additionally, in the cycled full cells with the ALD–TiO_2-20 electrodes, we observed much less transition metals on the graphite anodes, compared to the cells with the ALD–TiO_2-0 electrodes. In addition, XRD (X-ray diffraction) analysis revealed less cation mixing with the cycled ALD–TiO_2-20 electrodes than with the ALD–TiO_2-0 electrodes. Furthermore, the ALD–TiO_2-0 electrodes showed less voltage fading, which implied less formation of the electrochemically inactive NiO-type phase during cycling. All these observations verified that the ALD–TiO_2 coating is very beneficial for enhancing the performance of the NMC electrodes.

4.1.2 Al_2O_3 coating by ALD. Al_2O_3 is another popular ALD-resultant coating used for modifying NMC cathodes, including NMC111,[102] NMC532,[103] and NMC811.[104] We systematically investigated the effects of various coating thicknesses of ALD–Al_2O_3 on NMC 622 electrodes, namely, ALD–Al_2O_3-*X* (where *X* = 0, 10, 20, and 40 ALD cycles). The ALD–Al_2O_3 was deposited using trimethylaluminum (TMA) and water as the precursors at 100 °C, having a GPC of ~1.0 Å $cycle^{-1}$. Consequently, the coating thicknesses for the ALD–Al_2O_3-10, ALD–Al_2O_3-20, and ALD–Al_2O_3-40 cathodes were ~1, 2, and 4 nm, respectively. We confirmed that regardless of the thickness (1, 2, and 4 nm), all the ALD–Al_2O_3 coatings improved the capacity retention of NMC622 cathodes when applied to different upper cut-off voltages (4.3, 4.5, and 4.7 V *versus* Li/Li^+ for half-cells) (Fig. 6c-i–iii). The ALD–Al_2O_3-20 cathodes are optimal. Particularly, the underlying protection mechanism of the ALD–Al_2O_3 coatings is like that of the ALD–TiO_2 coatings.

4.1.3 ZrO_2 coating by ALD. In addition to TiO_2 and Al_2O_3, we also investigated ZrO_2 as a coating over the NMC622 cathodes. The ZrO_2 was deposited with ALD at 100 °C using TDMA-Zr and water as precursors; a GPC of ~1.6 Å $cycle^{-1}$ was observed.[79] Again, we varied the coating thicknesses of the ALD-resultant ZrO_2 coating, namely, ALD–ZrO_2-*X* (where *X* = 0, 5, 20, and 40 ALD cycles) (Fig. 6d). As expected, we confirmed the beneficial effects of the ALD–ZrO_2 coatings on the improved performance of NMC622 cathodes, in terms of cyclability, sustainable capacity, and rate capability, while the ALD–ZrO_2-20 cathodes (having a ZrO_2 coating of ~3.2 nm) exhibited the most notable enhancement. The underlying protection mechanism was also similar to that for TiO_2 and Al_2O_3.

4.2 ALD of lithium metal oxides

While Li-free metal oxides protected the NMC cathodes with improved performance, their low ionic conductivity limited their benefits. To this end, we studied Li-containing coatings as alternatives on the NMC cathodes,[83] showing better ionic conductivity than their Li-free counterparts. In the past decade, several Li-containing coatings have been reported to modify LIB cathodes, such as $LiAlO_2$,[85,105] $LiTaO_3$,[106] $LiAlF_4$,[87] Li_3PO_4,[107] and LiPON.[108] Our recent effort developed Li_xZr_yO (LZOs),[83] for which two sub-ALD processes of LiOH and ZrO_2 were combined to constitute a super-ALD process for LZOs. These sub-ALD processes have been reported previously.[23,109,110] The resultant super-ALD process for LZOs could deposit LZO by tuning the sub-ALD cycle ratio (*e.g.*, 1 : 1 and 1 : 2). We studied the effects of 1 : 1 LZO (1 : 1 is the sub-cycle ratio of the sub-ALD of LiOH and ZrO_2) on NMC622. Fig. 7a illustrates the initial charge–discharge profile of the coatings with various thicknesses of the ALD–LZO-*X*-coated NMC622 electrodes (where *X* = 0, 10, 20, 40, and 60 ALD cycles) of the 1 : 1 ALD–LZO samples. The GPC of the 1 : 1 ALD–LZO is ~1.1 Å super-$cycle^{-1}$ at a deposition

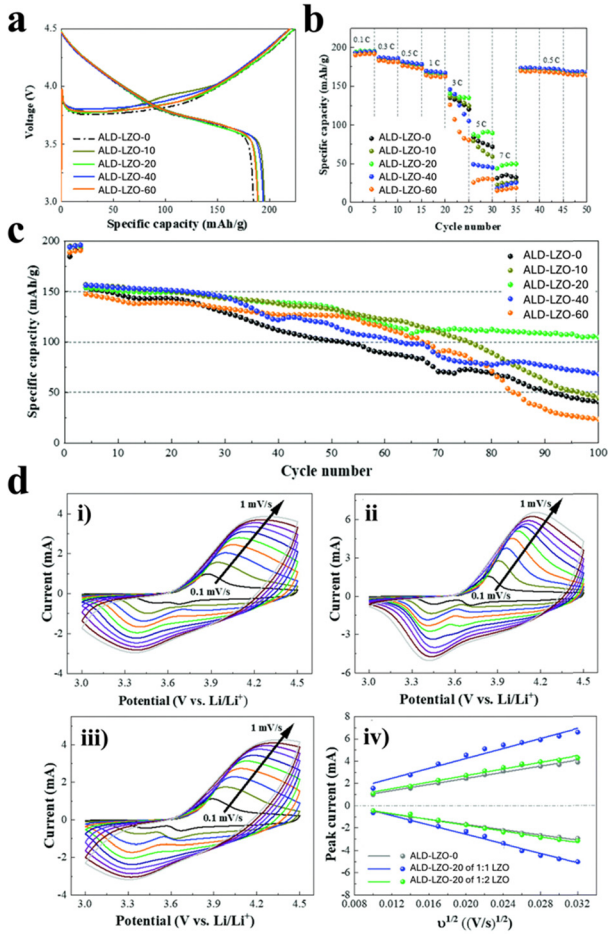

Fig. 7 Effects of the ALD–LZO coatings on the electrochemical performance of NMC622 cathodes in the range of 3.0–4.5 V. (a) Charge/discharge profile of bare and LZO-coated NMC cathodes; (b) C-rate (1C = 180 mA h g^{-1}), (c) long-term cyclability at 3C, and (d) CV measurements of different cathodes: (i) ALD–LZO-0, (ii) 1 : 1 ALD–LZO-20, and (iii) 1 : 2 ALD–LZO-20 at different scan rates (0.1–1.0 mV s^{-1} with a constant interval of 0.1 mV s^{-1}), and (iv) the linear relationship between maximum peak current *vs.* $\upsilon^{1/2}$. Adapted with permission from ref. 83. Copyright 2022, Royal Society of Chemistry. Note all electrochemical tests were performed within the voltage range of 3.0–4.5 V.

temperature of 225 °C. Electrochemical testing of the ALD–LZO-10 electrode revealed the highest specific discharge capacity of ~195, compared to the ALD–LZO-0 which has the lowest one of ~184 mA h g^{-1} (Fig. 7a). However, the rate capability of ALD–LZO-*X* (Fig. 7b) illustrated that at lower densities (0.1–1C), not much change was observed in the specific capacities, but it became evident beyond 3C, 5C, and 7C. At higher C-rates, the ALD–LZO-20 cathode exhibited the highest value of specific discharge capacity. Furthermore, the cyclability up to 100 cycles also revealed that the ALD–LZO-20 could maintain the highest capacity retention of 68%, which was much higher than that of ALD–LZO-0 (24%), ALD–LZO-10, ALD–LZO-40, and ALD–LZO-60. Hence, based on the electrochemical performance, these results showed that ALD–LZO-20 coating (~2.2 nm thick) is optimal. Also, the ALD–LZO-20 coating developed on the NMC622 electrode allowed working with much lesser discharge voltage drop than ALD–LZO-0, demonstrating the advantages of this ALD–LZO coating to improve the mechanical integrity of the coated NMC622 cathode and mitigate interfacial reactions. This has been verified by our analysis using synchrotron-based transmission X-ray microscopy (TXM) on the ALD–LZO-0 and ALD–LZO-20 electrodes before and after 200 charge/discharge cycles. Furthermore, to confirm the impact of the ALD–LZO coatings on the lithium-ion kinetics of the NMC622 cathode, we performed cyclic voltammetry (CV) at different scan rates (0.1–1.0 mV s^{-1} with a constant interval of 0.1 mV s^{-1}) (Fig. 7d). To this end, both the 1 : 1 and 1 : 2 ALD–LZO-20-coated NMC 622 electrodes (1 : 2 LZO was deposited at 225 °C with a GPC of 1.2 Å super-$cycle^{-1}$) showed improved lithium-ion insertion/extraction diffusion coefficient by 3.4 and 2.6 times, respectively. The linear relationships between charge–discharge peak currents, I_P, and $\upsilon^{1/2}$ (square rate of the scan rate), are also presented in Fig. 7d-iv. Conclusively, the 1 : 1 ALD–LZO-20 coating showed remarkable enhancement in the overall electrochemical performance, improved lithium-ion diffusivity, enhanced mechanical integrity, and mitigated interfacial reactions.

4.3 ALD of sulfides

Despite extensive research on surface coatings documented in the literature, oxygen release from NMC lattices remains a serious issue, which poses a serious risk to the long-term cyclability of NMCs. In this respect, our recent discovery of sulfide coatings represents a breakthrough, which could tackle the oxygen release of NMCs.

Sulfides have not been investigated as coating materials in literature, probably due to their sensitivity to air and the difficulty of processing. Our group made the first attempt to synthesize Li_2S *via* ALD and apply it as a coating over prefabricated NMC811 electrodes.[91] The ALD–Li_2S coating was deposited at 150 °C utilizing LTB and H_2S as precursors, while the ALD system was integrated with an Ar-filled glove box. The resultant Li_2S-coated NMC811 electrodes were named ALD–Li_2S-*X* (where *X* = 0, 10, 20, and 40 ALD cycles). The GPC for the ALD–Li_2S was ~1.1 Å $cycle^{-1}$. The coating thickness for ALD–Li_2S-10, ALD–Li_2S-20, and ALD–Li_2S-40 were ~1.1, 2.2, and 4.4 nm, respectively, where ALD–Li_2S-0 is the uncoated sample. Our systematic electrochemical tests revealed that the ALD–Li_2S-20 electrode is optimal and enables the best electrochemical performance.

We hypothesized that, due to its air-sensitive nature, the amorphous Li_2S coating could react with oxygen released from NMC lattices and convert it into Li_xS_yO (such as Li_2SO_3 and Li_2SO_4) (see Fig. 8a). The biggest benefit of such a sulfide coating is that it can protect the electrolyte solvents from oxidation by scavenging oxygen. Furthermore, the resultant Li_xS_yO could remain as a coating to play additional protective roles, while enabling better ionic conductivity than that of the Li_2S coating. Our electrochemical tests verified the benefits of the Li_2S coating. Specifically, the ALD–Li_2S-20 electrode enabled a longer cyclability than the ALD–Li_2S-0 electrode, *i.e.*, of up to 500 cycles at 0.5C for charge and 1C for discharge, as illustrated in Fig. 8b. The capacity retention was 71% for the

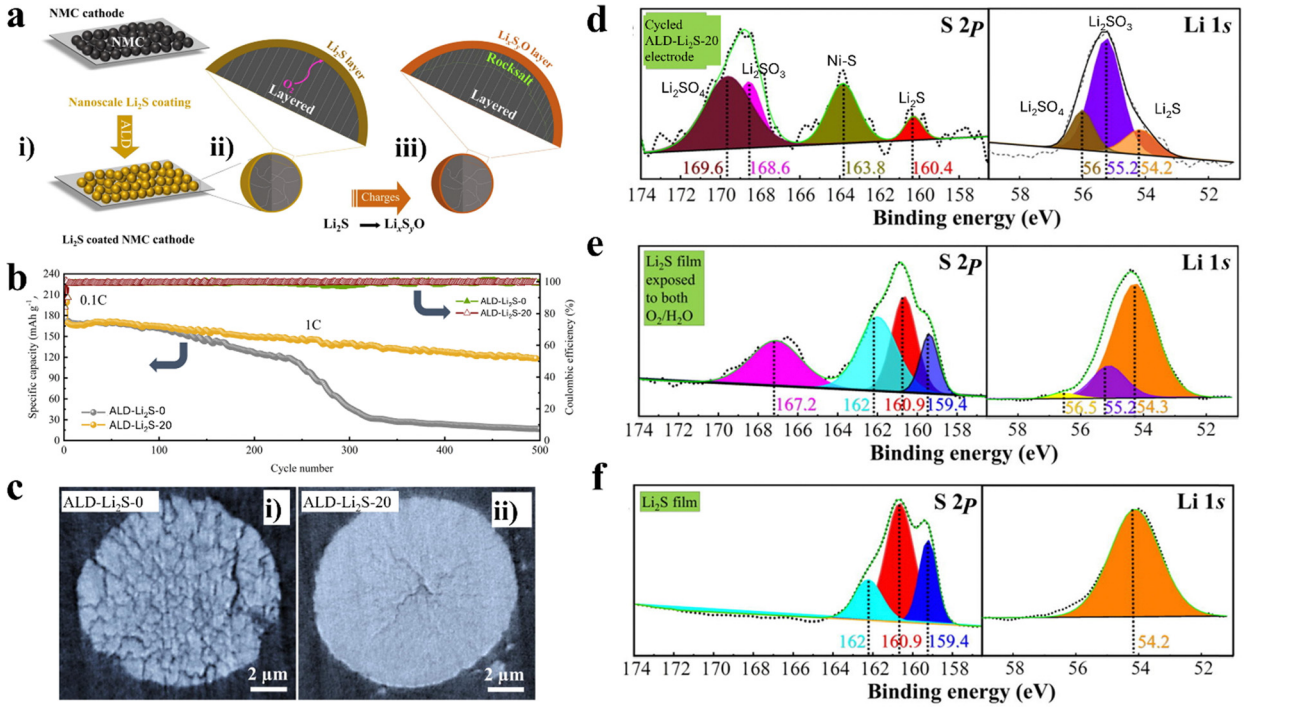

Fig. 8 The effects of ALD Li_2S coating on NMC811 cathode. (a) A schematic representation of protection and conversion mechanism of the Li_2S ALD coating on NMC811. (b) Long-term cyclability and Coulombic efficiency of bare and NMC811-Li_2S-20 cathodes, where the cells were charged/discharged at 0.5C/1C, respectively. (c) TXM images of NMC811 cathodes after 200 cycles: (i) uncoated and (ii) Li_2S-coated electrodes. High-resolution XPS spectra of S 2p and Li 1s for (d) cycled ALD–Li_2S-20 electrode after 20 cycles of charge (0.5C)/discharge (1C), (e) Li_2S film on Si wafer exposed to H_2O and O_2 for 30 min, and (f) pristine Li_2S film deposited on Si wafer. Adapted with permission from ref. 91. Copyright 2022, Journal of Energy Chemistry.

ALD–Li_2S-20 *versus* 11.6% for the ALD–Li_2S-0 electrode. Also, the synchrotron-based TXM study revealed that after 200 cycles (Fig. 8c), the NMC811 powder of the ALD–Li_2S-20 electrode did not show evident cracking, while the ALD–Li_2S-0 electrodes were extensively cracked.

Very importantly, we confirmed the conversion from Li_2S to Li_xS_yO based on XPS analysis (Fig. 8d). The cycled ALD–Li_2S-20 electrode was analyzed with XPS after 20 cycles of charge (0.5C)/discharge (1C), where the S 2p spectra showed peaks at 169.6 and 168.6 eV and Li 1s spectra exhibited peaks at 56 and 55.2 eV. These S 2p and Li 1s peaks were assigned to Li_2SO_4 and Li_2SO_3,[91] respectively. We also analyzed an ALD-resultant Li_2S film exposed to H_2O and O_2 for 30 min, which exhibited Li_2SO_3 and LiOH (Li 1s XPS peak at 56.5 and 55.2 eV) (Fig. 8e). Compared to Fig. 8d and e, the protected ALD–Li_2S film did not show any peaks attributable to Li_xS_yO and LiOH (Fig. 8f).

In summary, the ALD–Li_2S coating uncovered a new class of sulfide coating materials, which have not been explored and hold great promise for tackling the issues of NMCs. The benefits lie in multiple aspects: (1) protecting electrolyte solvents from oxidation; (2) mitigating electrode corrosion; (3) enhancing the mechanical integrity of both the NMC electrodes and powders; (4) stabilizing the electrode/electrolyte interface; and (5) minimizing irreversible structure and phase transitions of the NMCs. Consequently, this study is of great significance for NMCs and similar materials.

5. Li‖NMC full cells with integration of both ALD and MLD coatings

Following our progressive studies on ALD and MLD on Li anodes and NMC cathodes, we further investigated the synergistic effects of these ALD and MLD coatings on the resultant Li‖NMC LMBs.

5.1 LiTEA-200-coated Li‖Li_2S-20-coated NMC811

Our first attempt to integrate ALD and MLD coatings in Li‖NMC full cells was made with LiTEA-coated Li metal and Li_2S-coated NMC811. To this end, bare NMC811 and the Li_2S-20 electrodes were coupled with bare Li and LiTEA-200-coated Li electrodes; these setups were then tested in three cell configurations, *i.e.*, bare Li‖NMC811, LiTEA-200‖NMC811, and LiTEA-200‖Li_2S-20, at a voltage range of 3.0–4.3 V. Fig. 9a-i illustrates their distinct performance. To retain 80% capacity, specifically, the bare Li‖NMC811 cell survived 100 cycles and the LiTEA-200‖NMC811 cell extended to 150 cycles, while the LiTEA-200‖Li_2S-20 had a maximum cyclability of 210 cycles. After 80% capacity retention, in addition, the capacity dropping rates were very different, 0.92%, 0.63%, and 0.29% per cycle for the bare Li‖NMC811 cell, the LiTEA-200‖NMC811 cell, and the LiTEA-200‖Li_2S-20 cell. All these demonstrated that adopting both the MLD-LiTEA coating and the ALD–Li_2S coating could maximize the benefits to achieve the best

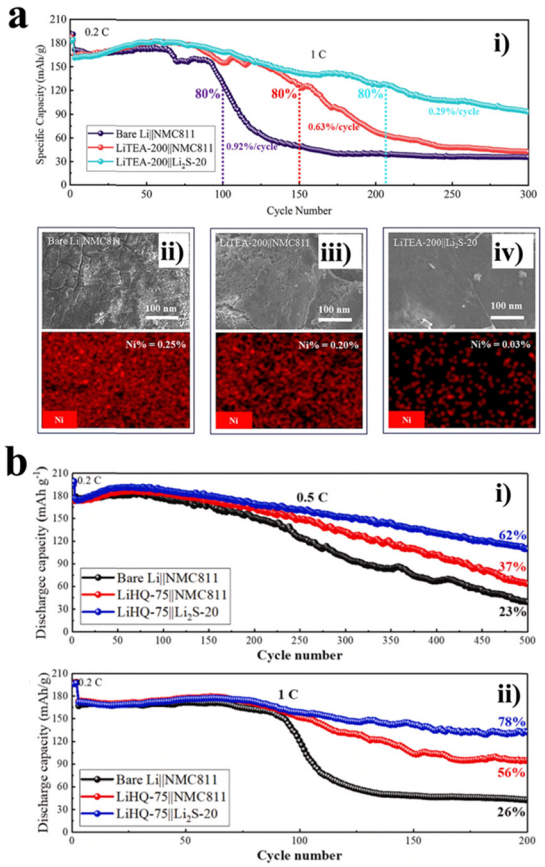

Fig. 9 Synergistic effects of the MLD-deposited LiTEA and LiHQ coatings and the ALD Li_2S coating on the resultant Li‖NMC811 cells. (a-i) Long-term cyclability of bare and ALD/MLD-coated Li‖NMC full cells, tested at 1C in the range of 3.0–4.3 V. SEM and EDX mapping for the cycled Li electrodes of (ii) bare Li‖NMC811, (iii) LiTEA-200‖NMC811, and (iv) LiTEA-200‖Li_2S-20 cells. Adapted with permission from ref. 54. Copyright 2023, Chemical Engineering Journal. (b) Tests of the long-term cyclability of bare Li‖NMC811, LiHQ-75‖NMC811, and LiHQ-75‖Li_2S-20 cells at (i) 0.5 and (ii) 1C for both charge and discharge cycles. Adapted with permission from ref. 53. Copyright 2024, Nano Energy.

electrochemical performance. These results have important implications. First, these two ALD and MLD coatings are compatible in the Li‖NMC811 cell. Second, they may mitigate the crosstalk between the Li anode and the NMC811 cathode. For the latter, we detected the presence of transition metals using energy-dispersive X-ray (EDX) spectroscopy, particularly Ni, on the cycled Li electrodes of these three cells after 300 cycles (Fig. 9a-ii–iv). It was found that the detected Ni contents were 0.25, 0.20, and 0.03 at% for the bare Li‖NMC811, LiTEA-200‖NMC811, and LiTEA-200‖Li_2S-20 cells, respectively. To pursue the best performance, thus, it is best to address the issues of both the Li anode and NMC cathode at the same time.

5.2 LiHQ-75-coated Li‖NMC811

We conducted another study on integrating both the MLD-LiHQ coatings and the ALD–Li_2S coating in Li‖NMC811 cells. As a result, three cell configurations were developed and tested, *i.e.*, bare Li‖NMC811, LiHQ-75-coated Li‖NMC811 (*i.e.*, LiHQ-75‖NMC811), and LiHQ-75-coated Li‖Li_2S-20-coated NMC811 (*i.e.*, LiHQ-75‖Li_2S-20). These full cells were cycled in a voltage window of 3.0–4.3 V at 0.5C (Fig. 9b-i) and 1C (Fig. 9b-ii) for both charge and discharge (where, 1C = 200 mA g^{-1}), followed by two formation cycles at 0.2C. Again, the Li‖NMC811 cells with both the ALD–Li_2S and MLD-LiHQ coatings (*i.e.*, LiHQ-75‖Li_2S-20) presented the best performance, followed by LiHQ-75‖NMC811 and bare Li‖NMC811. It is implied that these ALD and MLD coatings are compatible and synergistic in their beneficial effects.

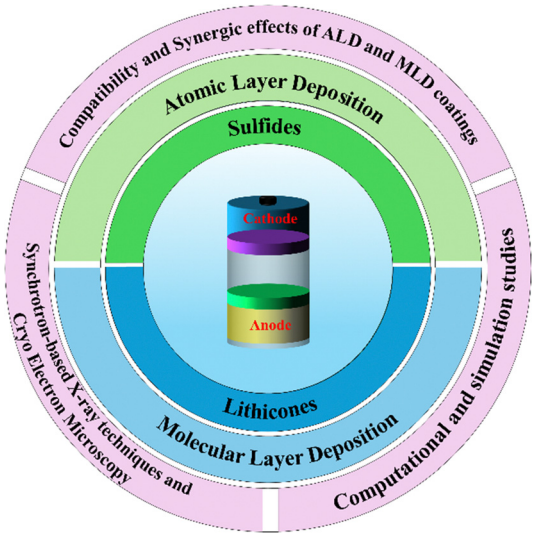

Fig. 10 More efforts are needed to develop new coatings and understand the interfaces in lithium metal batteries.

6. Conclusions and outlooks

ALD and MLD are two powerful techniques to search for new solutions for the next generation of emerging battery systems due to their unique capabilities for producing high-quality versatile coatings. This Feature Article provides a timely summary of our recent encouraging progress on ALD and MLD coatings for developing long-term stable high-energy Li‖NMC LMBs. Our contributions are mainly exhibited in three aspects: (1) novel polymeric lithicone coatings *via* MLD to tackle typical issues with Li anodes. (2) New inorganic coatings *via* ALD for addressing the issues of NMC cathodes. We particularly discuss the discovery of sulfides as a new class of coating materials. (3) These ALD and MLD-resultant coatings are compatible and could work synergistically for the best performance of Li‖NMC LMBs. Thus, these studies are very encouraging and inspiring.

Following these exciting studies, we should also realize that there are still many efforts needed urgently to develop Li‖NMC LMBs and similar products. First, as a new class of polymers, lithicones are not well understood and studied. We only reported three types of lithicones, and thus, more effort must be devoted to understanding their Li-diffusion mechanisms, and their mechanical, chemical, and electrochemical properties. Based on this knowledge, we may be able to design and develop

better alternatives *via* MLD. Second, sulfides as a new class of coatings materials exhibit unique functions that are not explored well. In addition to Li_2S, there is a large variety of other sulfides with varied properties. Some sulfides may be able to perform better as coatings in place of Li_2S and need further investigation. Third, the compatibility and synergistic effects of ALD and MLD coatings in Li‖NMC LMBs are very interesting and should be fully studied. In pursuing these goals, it is necessary to secure advanced characterizations, such as synchrotron-based X-ray techniques and cryoelectron microscopy (cryo-EM). Furthermore, the atomic simulations are also of great importance in providing insights into the roles of ALD and MLD coatings as shown in Fig. 10. Computational studies and simulations are essential for the advancement of ALD and MLD coatings for lithium anodes and cathode interfaces. Density functional theory (DFT)-enhanced computational fluid dynamics (CFD) modeling, for instance, provides valuable insights into precursor reactions, substrate movement, and deposition processes in ALD, enabling optimization of coating uniformity.[111] Advanced computational approaches have also been used to design cathode coatings for the identification of materials with enhanced ionic conductivity and interfacial stability.[112] Additionally, it is expected that interfaces will be analyzed by combining cryo-EM techniques with computational methods. Such a combination may provide insightful views on the SEI layer formation and interfacial dynamics of lithium metal anodes. Such knowledge will be essential to understand the relationship between interface and cell performance.[113] For MLD coatings, DFT simulations could help us understand lithium-ion diffusion mechanisms in lithicones, which will help further develop new polymeric coatings.[114]

Thus, it is encouraged to conduct a series of comprehensive interdisciplinary studies. To this end, we expect to make further progress in advancing our understanding of Li‖NMC LMBs and promote technical solutions.

Author contributions

K. V. C.: writing – original draft. M. S.: writing – original draft. X. M.: supervision, funding acquisition, project administration, writing – reviewing and editing.

Data availability

Data for this article, including experimental datasets, metrics for battery performance, and simulation results are available at our group website, **https://nano-energy-lab.uark.edu/publications/**.

Conflicts of interest

There are no conflicts to declare.

Acknowledgements

We acknowledge the support from the U.S. Department of Energy, Office of Science, Office of Basic Energy Sciences with the award number DE-SC0023439.

Notes and references

1 X. Meng, K. C. Lau, H. Zhou, S. K. Ghosh, M. Benamara and M. Zou, *Energy Mater. Adv.*, 2021, **2021**, 9786201.
2 R. Schmuch, R. Wagner, G. Hörpel, T. Placke and M. Winter, *Nat. Energy*, 2018, **3**, 267–278.
3 O. Schmidt, A. Hawkes, A. Gambhir and I. Staffell, *Nat. Energy*, 2017, **2**, 17110.
4 M. Singh, T. Dawsey and R. K. Gupta, *J. Energy Storage*, 2023, **73**, 109059.
5 J. Neubauer, A. Pesaran, B. A. E. Chulheung, R. Elder and B. Cunningham, *J. Power Sources*, 2014, **271**, 614–621.
6 Z. Li, N. Qin and Z. Lu, *Nat. Energy*, 2023, **8**, 321–322.
7 K. Yoon, S. Lee, K. Oh and K. Kang, *Adv. Mater.*, 2022, **34**, e2104666.
8 P. Albertus, V. Anandan, C. Ban, N. Balsara, I. Belharouak, J. Buettner-Garrett, Z. Chen, C. Daniel, M. Doeff, N. J. Dudney, B. Dunn, S. J. Harris, S. Herle, E. Herbert, S. Kalnaus, J. A. Libera, D. Lu, S. Martin, B. D. McCloskey, M. T. McDowell, Y. S. Meng, J. Nanda, J. Sakamoto, E. C. Self, S. Tepavcevic, E. Wachsman, C. Wang, A. S. Westover, J. Xiao and T. Yersak, *ACS Energy Lett.*, 2021, **6**, 1399–1404.
9 D. Lin, Y. Liu and Y. Cui, *Nat. Nanotechnol.*, 2017, **12**, 194–206.
10 P. G. Bruce, S. A. Freunberger, L. J. Hardwick and J. M. Tarascon, *Nat. Mater.*, 2012, **11**, 19–29.
11 X.-B. Cheng, R. Zhang, C.-Z. Zhao and Q. Zhang, *Chem. Rev.*, 2017, **117**, 10403–10473.
12 P. Selinis and F. Farmakis, *J. Electrochem. Soc.*, 2022, **169**, 10526.
13 E. Peled and S. Menkin, *J. Electrochem. Soc.*, 2017, **164**, A1703–A1719.
14 X. Zhang, A. Wang, X. Liu and J. Luo, *Acc. Chem. Res.*, 2019, **52**, 3223–3232.
15 H. Zhang, G. G. Eshetu, X. Judez, C. Li, L. M. Rodriguez-Martínez and M. Armand, *Angew. Chem., Int. Ed.*, 2018, **57**, 15002–15027.
16 X. R. Wang and G. Yushin, *Energy Environ. Sci.*, 2015, **8**, 1889–1904.
17 B. Uzakbaiuly, A. Mukanova, Y. G. Zhang and Z. Bakenov, *Front. Energy Res.*, 2021, **9**, 625123.
18 X. Meng, *Inorg. Chem. Front.*, 2024, **11**, 659–681.
19 X. Meng, *J. Mater. Res.*, 2021, **36**, 2–25.
20 Y. Liu, X. Wang, J. Cai, X. Han, D. Geng, J. Li and X. Meng, *J. Mater. Sci. Technol.*, 2020, **54**, 77–86.
21 X. Wang, S. K. Ghosh, M. Afshar-Mohajer, H. Zhou, Y. Liu, X. Han, J. Cai, M. Zou and X. Meng, *J. Mater. Res.*, 2020, **35**, 804–812.
22 J. Liu, X. Meng, Y. Hu, D. Geng, M. N. Banis, M. Cai, R. Li and X. Sun, *Carbon*, 2013, **52**, 74–82.
23 J. Liu, X. Meng, M. N. Banis, M. Cai, R. Li and X. Sun, *J. Phys. Chem. C*, 2012, **116**, 14656–14664.
24 W. Xu, J. Wang, F. Ding, X. Chen, E. Nasybulin, Y. Zhang and J.-G. Zhang, *Energy Environ. Sci.*, 2014, **7**, 513–537.
25 B. Liu, J.-G. Zhang and W. Xu, *Joule*, 2018, **2**, 833–845.
26 W. Liu, P. Liu and D. Mitlin, *Adv. Energy Mater.*, 2020, **10**, 2002297.
27 Y. Cheng, Z. Wang, J. Chen, Y. Chen, X. Ke, D. Wu, Q. Zhang, Y. Zhu, X. Yang, M. Gu, Z. Guo and Z. Shi, *Angew. Chem., Int. Ed.*, 2023, **62**, e202305723.
28 H. Zhou, H. M. Li, Q. Gong, S. Yan, X. B. Zhou, S. Z. Liang, W. J. Ding, Y. L. He, K. Jiang and K. L. Wang, *Energy Storage Mater.*, 2022, **50**, 572–579.
29 Q. Zhang, Y. Y. Lu, L. C. Miao, Q. Zhao, K. X. Xia, J. Liang, S. L. Chou and J. Chen, *Angew. Chem., Int. Ed.*, 2018, **57**, 14796–14800.
30 E. Peled, *J. Electrochem. Soc.*, 1979, **126**, 2047–2051.
31 J. X. Li, J. N. Liang, Z. H. Ren, C. Shi, Y. L. Li, L. Zhang, Q. L. Zhang, C. X. He and X. Z. Ren, *Electrochim. Acta*, 2022, **429**, 141061.
32 X. Gao, Y.-N. Zhou, D. Han, J. Zhou, D. Zhou, W. Tang and J. B. Goodenough, *Joule*, 2020, **4**, 1864–1879.
33 K. Nishikawa, T. Mori, T. Nishida, Y. Fukunaka and M. Rosso, *J. Electroanal. Chem.*, 2011, **661**, 84–89.

34 Y. Xiang, M. Tao, G. Zhong, Z. Liang, G. Zheng, X. Huang, X. Liu, Y. Jin, N. Xu, M. Armand, J.-G. Zhang, K. Xu, R. Fu and Y. Yang, *Sci. Adv.*, 2021, **7**, eabj3423.
35 F. Sun and I. Manke, *ChemElectroChem*, 2019, **6**, 5787–5789.
36 L. Wang, A. Menakath, F. Han, Y. Wang, P. Y. Zavalij, K. J. Gaskell, O. Borodin, D. Iuga, S. P. Brown, C. Wang, K. Xu and B. W. Eichhorn, *Nat. Chem.*, 2019, **11**, 789–796.
37 C. Fang, J. Li, M. Zhang, Y. Zhang, F. Yang, J. Z. Lee, M.-H. Lee, J. Alvarado, M. A. Schroeder, Y. Yang, B. Lu, N. Williams, M. Ceja, L. Yang, M. Cai, J. Gu, K. Xu, X. Wang and Y. S. Meng, *Nature*, 2019, **572**, 511–515.
38 D. T. Boyle, W. Huang, H. Wang, Y. Li, H. Chen, Z. Yu, W. Zhang, Z. Bao and Y. Cui, *Nat. Energy*, 2021, **6**, 487–494.
39 X. B. Cheng, R. Zhang, C. Z. Zhao, F. Wei, J. G. Zhang and Q. Zhang, *Adv. Sci.*, 2016, **3**, 1500213.
40 R. Khurana, J. L. Schaefer, L. A. Archer and G. W. Coates, *J. Am. Chem. Soc.*, 2014, **136**, 7395–7402.
41 J. M. Zheng, M. H. Engelhard, D. H. Mei, S. H. Jiao, B. J. Polzin, J. G. Zhang and W. Xu, *Nat. Energy*, 2017, **2**, 17012.
42 M. Xia, M. Lin, G. Liu, Y. Cheng, T. Jiao, A. Fu, Y. Yang, M. Wang and J. Zheng, *Chem. Eng. J.*, 2022, **442**, 136351.
43 K.-H. Chen, A. J. Sanchez, E. Kazyak, A. L. Davis and N. P. Dasgupta, *Adv. Energy Mater.*, 2019, **9**, 1802534.
44 Y. Zhang, B. Liu, E. Hitz, W. Luo, Y. Yao, Y. Li, J. Dai, C. Chen, Y. Wang, C. Yang, H. Li and L. Hu, *Nano Res.*, 2017, **10**, 1356–1365.
45 J. Lopez, D. G. Mackanic, Y. Cui and Z. Bao, *Nat. Rev. Mater.*, 2019, **4**, 312–330.
46 Z. Yu, D. G. Mackanic, W. Michaels, M. Lee, A. Pei, D. Feng, Q. Zhang, Y. Tsao, C. V. Amanchukwu, X. Yan, H. Wang, S. Chen, K. Liu, J. Kang, J. Qin, Y. Cui and Z. Bao, *Joule*, 2019, **3**, 2761–2776.
47 Y. Liu, Y.-K. Tzeng, D. Lin, A. Pei, H. Lu, N. A. Melosh, Z.-X. Shen, S. Chu and Y. Cui, *Joule*, 2018, **2**, 1595–1609.
48 Y. Zhao, M. Amirmaleki, Q. Sun, C. T. Zhao, A. Codirenzi, L. V. Goncharova, C. H. Wang, K. Adair, X. Li, X. F. Yang, F. P. Zhao, R. Y. Li, T. Filleter, M. Cai and X. L. Sun, *Matter*, 2019, **1**, 1215–1231.
49 E. Kazyak, K. N. Wood and N. P. Dasgupta, *Chem. Mater.*, 2015, **27**, 6457–6462.
50 A. C. Kozen, C.-F. Lin, A. J. Pearse, M. A. Schroeder, X. Han, L. Hu, S.-B. Lee, G. W. Rubloff and M. Noked, *ACS Nano*, 2015, **9**, 5884–5892.
51 Y. Q. Cao, X. B. Meng and J. W. Elam, *ChemElectroChem*, 2016, **3**, 858–863.
52 R. A. Ahmed, K. V. Carballo, K. P. Koirala, Q. Zhao, P. Gao, J. M. Kim, C. S. Anderson, X. Meng, C. Wang, J. G. Zhang and W. Xu, *Small Struct.*, 2024, **5**, 2400174.
53 X. Wang, K. V. Carballo, A. Shao, J. Cai, F. Watanabe and X. Meng, *Nano Energy*, 2024, **128**, 109840.
54 X. Wang, J. Cai, K. Velasquez Carballo, F. Watanabe and X. Meng, *Chem. Eng. J.*, 2023, **475**, 146156.
55 M. Wang, X. Cheng, T. Cao, J. Niu, R. Wu, X. Liu and Y. Zhang, *J. Alloys Compd.*, 2021, **865**, 158748.
56 P. K. Alaboina, S. Rodrigues, M. Rottmayer and S.-J. Cho, *ACS Appl. Mater. Interfaces*, 2018, **10**, 32801–32808.
57 J. Niu, M. Wang, T. Cao, X. Cheng, R. Wu, H. Liu, Y. Zhang and X. Liu, *Ionics*, 2021, **27**, 2445–2454.
58 F. Huang, P. Xu, G. Fang and S. Liang, *Adv. Mater.*, 2024, **36**, 2405310.
59 P. Xu, F. Huang, Y. Sun, Y. Lei, X. Cao, S. Liang and G. Fang, *Adv. Funct. Mater.*, 2024, **34**, 2406080.
60 S. Passerini, L. Barelli, M. Baumann, J. Peters and M. Weil, *Emerging Battery Technologies to Boost the Clean Energy Transition: Cost, Sustainability, and Performance Analysis*, Springer International Publishing, Cham, 1st edn, 2024, vol. 2024.
61 S. C. Jung and Y.-K. Han, *J. Phys. Chem. Lett.*, 2013, **4**, 2681–2685.
62 R. Gover, J. Tolchard, H. Tukamoto, T. Murai and J. Irvine, *J. Electrochem. Soc.*, 1999, **146**, 4348–4353.
63 R. Götz, E. Pugacheva, Z. Ahaliabadeh, P. S. S. Llanos, T. Kallio and A. Bandarenka, *ChemSusChem*, 2024, e202401026, DOI: **10.1002/cssc.202401026**.
64 Y. Sun, Y. Zhao, J. Wang, J. Liang, C. Wang, Q. Sun, X. Lin, K. R. Adair, J. Luo, D. Wang, R. Li, M. Cai, T. K. Sham and X. Sun, *Adv. Mater.*, 2019, **31**, e1806541.
65 Y. Zhao, L. V. Goncharova, Q. Sun, X. Li, A. Lushington, B. Wang, R. Li, F. Dai, M. Cai and X. Sun, *Small Methods*, 2018, **2**, 1700417.
66 L. Chen, Z. Huang, R. Shahbazian-Yassar, J. A. Libera, K. C. Klavetter, K. R. Zavadil and J. W. Elam, *ACS Appl. Mater. Interfaces*, 2018, **10**, 7043–7051.
67 K. R. Adair, C. Zhao, M. N. Banis, Y. Zhao, R. Li, M. Cai and X. Sun, *Angew. Chem., Int. Ed.*, 2019, **58**, 15797–15802.
68 S. Park, R. Chaudhary, S. A. Han, H. Qutaish, J. Moon, M.-S. Park and J. H. Kim, *Energy Mater.*, 2023, **3**, 300005.
69 N. Yang, X.-Q. Xu and J.-X. Zheng, *Phys. Rev. Mater.*, 2024, **8**, 015403.
70 J. Langdon and A. Manthiram, *Adv. Funct. Mater.*, 2021, **31**, 2010267.
71 H. Lee, H.-S. Lim, X. Ren, L. Yu, M. H. Engelhard, K. S. Han, J. Lee, H.-T. Kim, J. Xiao, J. Liu, W. Xu and J.-G. Zhang, *ACS Energy Lett.*, 2018, **3**, 2921–2930.
72 X. Meng, *Energy Storage Mater.*, 2020, **30**, 296–328.
73 X. Meng, X.-Q. Yang and X. Sun, *Adv. Mater.*, 2012, **24**, 3589–3615.
74 S.-T. Myung, K. Izumi, S. Komaba, Y.-K. Sun, H. Yashiro and N. Kumagai, *Chem. Mater.*, 2005, **17**, 3695–3704.
75 W. Liu, X. Li, D. Xiong, Y. Hao, J. Li, H. Kou, B. Yan, D. Li, S. Lu, A. Koo, K. Adair and X. Sun, *Nano Energy*, 2018, **44**, 111–120.
76 H. Gao, J. Cai, G.-L. Xu, L. Li, Y. Ren, X. Meng, K. Amine and Z. Chen, *Chem. Mater.*, 2019, **31**, 2723–2730.
77 D. Becker, M. Börner, R. Nölle, M. Diehl, S. Klein, U. Rodehorst, R. Schmuch, M. Winter and T. Placke, *ACS Appl. Mater. Interfaces*, 2019, **11**, 18404–18414.
78 F. Tao, X.-X. Yan, J.-J. Liu, H.-L. Zhang and L. Chen, *Electrochim. Acta*, 2016, **210**, 548–556.
79 Y. Q. Liu, X. Wang, J. Y. Cai, X. X. Han, D. S. Geng, J. L. Li and X. B. Meng, *J. Mater. Sci. Technol.*, 2020, **54**, 77–86.
80 J.-Z. Kong, C. Ren, G.-A. Tai, X. Zhang, A.-D. Li, D. Wu, H. Li and F. Zhou, *J. Power Sources*, 2014, **266**, 433–439.
81 G. R. Hu, Y. Tao, Y. Lu, J. Fan, L. Y. Li, J. Xia, Y. Huang, Z. Y. Zhang, H. D. Su and Y. B. Cao, *ChemElectroChem*, 2019, **6**, 4773–4780.
82 H. Liang, Z. Wang, H. Guo, J. Wang and J. Leng, *Appl. Surf. Sci.*, 2017, **423**, 1045–1053.
83 Y. Q. Liu, X. Wang, S. K. Ghosh, M. Zou, H. Zhou, X. H. Xiao and X. B. Meng, *Dalton Trans.*, 2022, **51**, 2737–2749.
84 I. Bloom, L. Trahey, M. Xiangbo, A. K. Burrell, B. A. N. Chunmei, R. Tenent, J. Nanda, N. Dudney, A. Abouimrane, I. Belharouak, Z. Xiaofeng, W. U. Qingliu, L. U. Wenquan, D. P. Abraham, M. Bettge and J. W. Elam, *J. Power Sources*, 2014, **249**, 509–514.
85 J. S. Park, X. Meng, J. W. Elam, S. Hao, C. Wolverton, C. Kim and J. Cabana, *Chem. Mater.*, 2014, **26**, 3128–3134.
86 Y.-D. Xu, W. Xiang, Z.-G. Wu, C.-L. Xu, Y.-C. Li, X.-D. Guo, G.-P. Lv, X. Peng and B.-H. Zhong, *Electrochim. Acta*, 2018, **268**, 358–365.
87 J. Xie, A. D. Sendek, E. D. Cubuk, X. Zhang, Z. Lu, Y. Gong, T. Wu, F. Shi, W. Liu, E. J. Reed and Y. Cui, *ACS Nano*, 2017, **11**, 7019–7027.
88 Z. Chen, G. T. Kim, D. Bresser, T. Diemant, J. Asenbauer, S. Jeong, M. Copley, R. J. Behm, J. Lin, Z. Shen and S. Passerini, *Adv. Energy Mater.*, 2018, **8**, 1801573.
89 S. Dai, G. Yan, L. Wang, L. Luo, Y. Li, Y. Yang, H. Liu, Y. Liu and M. Yuan, *J. Electroanal. Chem.*, 2019, **847**, 113197.
90 X. Xiong, Z. Wang, X. Yin, H. Guo and X. Li, *Mater. Lett.*, 2013, **110**, 4–9.
91 X. Wang, J. Cai, Y. Ren, M. Benamara, X. Zhou, Y. Li, Z. Chen, H. Zhou, X. Xiao, Y. Liu and X. Meng, *J. Energy Chem.*, 2022, **69**, 531–540.
92 X. Meng, M. N. Banis, D. Geng, X. Li, Y. Zhang, R. Li, H. Abou-Rachid and X. Sun, *Appl. Surf. Sci.*, 2013, **266**, 132–140.
93 X. Meng, D. S. Geng, J. A. Liu, R. Y. Li and X. L. Sun, *Nanotechnology*, 2011, **22**, 165602.
94 M. Li, X. Li, W. Li, X. Meng, Y. Yu and X. Sun, *Electrochem. Commun.*, 2015, **57**, 43–47.
95 D. M. King, L. Xinhua, Z. Yun, C. S. Carney, L. F. Hakim, L. I. Peng and A. W. Weimer, *Powder Technol.*, 2008, **183**, 356–363.
96 J. D. Ferguson, A. R. Yoder, A. W. Weimer and S. M. George, *Appl. Surf. Sci.*, 2004, **226**, 393–404.
97 H. Shin, D. K. Jeong, J. Lee, M. M. Sung and J. Kim, *Adv. Mater.*, 2004, **16**, 1197–1200.
98 M. Knez, K. Nielsch and L. Niinistö, *Adv. Mater.*, 2007, **19**, 3425–3438.
99 Eksergi, DOI: **10.31315/e.v17i2.3714**.

100 X. D. Wang, E. Graugnard, J. S. King, Z. L. Wang and C. J. Summers, *Nano Lett.*, 2004, **4**, 2223–2226.
101 X. Wang, J. Y. Cai, Y. Q. Liu, X. X. Han, Y. Ren, J. L. Li, Y. Z. Liu and X. B. Meng, *Nanotechnology*, 2021, **32**, 115401.
102 L. A. Riley, S. Van Atta, A. S. Cavanagh, Y. Yan, S. M. George, P. Liu, A. C. Dillon and S.-H. Lee, *J. Power Sources*, 2011, **196**, 3317–3324.
103 Y. Shi, M. H. Zhang, D. N. Qian and Y. S. Meng, *Electrochim. Acta*, 2016, **203**, 154–161.
104 W. Zhu, X. Huang, T. Liu, Z. Xie, Y. Wang, K. Tian, L. Bu, H. Wang, L. Gao and J. Zhao, *Coatings*, 2019, **9**, 92.
105 I. Bloom, L. Trahey, A. Abouimrane, I. Belharouak, X. Zhang, Q. Wu, W. Lu, D. Abraham, M. Bettge, J. Elam, X. Meng, A. Burrell, C. Ban, R. Tenent, J. Nanda and N. Dudney, *J. Power Sources*, 2014, **249**, 509–514.
106 X. Li, J. Liu, M. N. Banis, A. Lushington, R. Li, M. Cai and X. Sun, *Energy Environ. Sci.*, 2014, **7**, 768–778.
107 P. F. Yan, J. M. Zheng, J. Liu, B. Q. Wang, X. P. Cheng, Y. F. Zhang, X. L. Sun, C. M. Wang and J. G. Zhang, *Nat. Energy*, 2018, **3**, 600–605.
108 C.-F. Lin, X. Fan, A. Pearse, S.-C. Liou, K. Gregorczyk, M. Leskes, C. Wang, S. B. Lee, G. W. Rubloff and M. Noked, *Chem. Mater.*, 2017, **29**, 8780–8791.
109 X. Wang, S. Ghosh, M. Afshar-Mohajer, H. Zhou, Y. Q. Liu, X. X. Han, J. Y. Cai, M. Zou and X. B. Meng, *J. Mater. Res.*, 2020, **35**, 804–812.
110 S. C. Andrew, L. Younghee, Y. Byunghoon and M. G. Steven, *ECS Trans.*, 2010, **33**, 223–229.
111 R. L. Puurunen, *Chem. Vap. Deposition*, 2014, **20**, 332–344.
112 M. Aykol, S. Kim, V. I. Hegde, D. Snydacker, Z. Lu, S. Hao, S. Kirklin, D. Morgan and C. Wolverton, *Nat. Commun.*, 2016, **7**, 13779.
113 P. Zhai, L. Liu, X. Gu, T. Wang and Y. Gong, *Adv. Energy Mater.*, 2020, **10**, 2001257.
114 D. Pan, *Chem. Eng. Sci.*, 2021, **234**, 116447.